T H E U N I V E R S I T Y O F M I C H I G A N

COLLEGE OF ENGINEERING
Department of Aeronautical and Astronautical Engineering
High Altitude Engineering Laboratory

Technical Report

ATMOSPHERIC SOUNDING BY SATELLITE MEASUREMENTS OF STELLAR REFRACTION

F. F. Fischbach
M. E. Graves
P. B. Hays
G. S. Klein
C. M. Mizgala
J. W. Peterson

ORA Project 04963

under contract with:

NATIONAL AERONAUTICS AND SPACE ADMINISTRATION
GODDARD SPACE FLIGHT CENTER
CONTRACT NO. NASw-140
GREENBELT, MARYLAND

administered through:

OFFICE OF RESEARCH ADMINISTRATION ANN ARBOR

December 1962

TABLE OF CONTENTS

TABLE OF CONTENTS (Concluded)

LIST OF TABLES

LIST OF FIGURES

LIST OF FIGURES (Concluded)

PARTIAL LIST OF SYMBOLS

b	departure of refracted ray at tangency from an unrefracted ray
g	gravitational acceleration
GP	geographical position (longitude and latitude) of a satellite or light ray tangency
h	altitude above the earth's surface
H	scale height
M	mean molecular weight
p	atmospheric pressure
r	radius from center of the earth
R	refraction angle
R*	universal gas constant
r_e	earth's radius = 6371 km
s	distance along a ray path
T	atmospheric temperature
z	zenith angle

Greek Letters

β	latitude
γ	vernal equinox (Aries)
μ	index of refraction
ν	refractivity = μ-1
ρ	atmospheric density

PARTIAL LIST OF SYMBOLS (Concluded)

Subscripts

L	in the horizontal plane, lateral to the ray
o	at light ray tangency to the earth, or to a spherically stratified atmospheric shell
P	in the plane of the refracted ray
s	as measured on the satellite, or to the satellite position

THE UNIVERSITY OF MICHIGAN PROJECT PERSONNEL

Both Full and Part Time

Bodine, Margie S., Secretary

Childs, David L., B.S.E., Assistant in Research

Fischbach, Frederick F., M.S., Associate Research Mathematician

Graves, Maurice E., S.M., Assistant Research Meteorologist

Hays, Paul B., M.S.E., Assistant in Research

Jones, Leslie M., B.S.E., Laboratory Director

Klein, Gretchen S., B.S., Assistant in Research

Mizgala, Charles M., B.S., Assistant in Research

Mosakewicz, Mary C., Secretary

Peterson, John W., M.S., Associate Research Engineer

ABSTRACT

A method of obtaining atmospheric density, temperature, and pressure profiles between 5 and 25 km by measuring the refraction of stellar images with satellite instrumentation is described. The daily location of observations over the earth's surface which may be obtained from a Nimbus-type orbit is shown. Instrumentation and data handling requirements are outlined. Current areas under investigation are described.

ACKNOWLEDGEMENT

The authors gratefully acknowledge the financial support of the Aeronomy and Meteorology Branch, Goddard Space Flight Center, NASA, which made the project possible.

The Baker-Nunn ballistic camera measurements were made with the cooperation of the crew of the Smithsonian Satellite Tracking Station, Maui, especially Messrs. J. T. Williams and William Perry. A great amount of credit also goes to the Smithsonian Astrophysical Observatory personnel in Cambridge, whose generous support of the project has ranged from permission to use their camera to assistance with the data reduction.

I. INTRODUCTION

This is the second report on the refractive technique for atmospheric structure measurements. Several basic ideas have been revised, corrected, and augmented since the first report,[1,2] and because it is deemed important that the technique be fully described within a single binding, a certain amount of background material and the fundamentals are reiterated herein. The reader is assured that the present report contains a comprehensive picture of the technique to date.

An orbiting vehicle with the means of viewing stars through the earth's atmosphere and of measuring the refraction of the starlight permits deduction of the density, temperature, and pressure of the atmosphere at perigee of the light ray. The limits are approximately 5 km to 25 km, the lower limit due to probable obscuration of the light ray by clouds and the upper limit due to diminution of the effect to be measured. The refraction is a direct measure of density as given in the Dale and Gladstone Law, $\nu = k\rho$, where ν is refractivity and ρ is atmospheric density. Since the orbiting equipment can measure only the total refraction of a ray and there are contributions to refraction by varying densities along the ray path, the means of ascribing the measurement to the perigee location is given. As a particular star is viewed during occulation by the earth, several measurements may be made at different ray heights; thus a density profile is obtained, permitting integration for pressure and temperature structure as well.

The time required for a profile is found to be less than 30 seconds, and with a pair of telescopes sufficient measurements may be made to approach an observation density of one profile every 200 miles over the earth's surface. Only a little more than 10^5 information bits per orbit are required from telemetry. Data processing in time equal to observation time is required to prevent backlogging of data and might be handled by one IBM 7090 computer.

Data reduction requires precise satellite tracking which exceeds present capabilities, but which is anticipated to be available within a year or two. Other requirements appear to be within present capabilities.

It should be noted that the refraction technique attacks the meteorological problem by furnishing the data meteorologists are presently equipped to handle: pressure, temperature, and density. To accomplish this requires development of the refraction measuring equipment. This stands in sharp contrast to the current use of television pictures and infrared radiation measurements, which utilize proven equipment and methods but require meteorologists to develop new techniques in forecasting.

Neither approach can be called correct or incorrect. Nor does one in any way degrade the value of the other; in fact, cloud photographs in addition to p, t, ρ, profiles would place the forecaster in a very strong position. However, the information rate required for the refractive technique is only about 2% of the others, indicating the great directness of this technique in measuring atmospheric structure.

II. THE THEORETICAL BASIS FOR A SINGLE DENSITY PROFILE

A. ASTRONOMICAL REFRACTION

When a ray of light passes through a medium of varying refractive index, μ, it undergoes a curvature C where

$$C = \frac{\text{grad } \mu}{\mu} \sin z \,. \tag{1}$$

Here z is the angle between the ray and the gradient; but the gradient lies along an earth's radius, making z the zenith angle. If a stellar ray enters the atmosphere on any oblique path, its integrated curvature when it reaches an observer is known as the refraction angle, thus:

$$R_o = \int C ds \tag{2}$$

In the case of a ray entering a spherically stratified atmosphere, Eq. (2) becomes

$$R_o = \int_1^{\mu_o} \frac{d\mu}{\mu} \tan z \tag{2a}$$

Snell's law for a spherically stratified atmosphere provides the equation

$$\mu r \sin z = \text{const.} \tag{3}$$

where r is the radius of curvature of the strata, a function of the altitude h. Equation (2a) then becomes

$$R_o = \mu_o r_o \sin z_o \int_1^{\mu_o} \frac{d\mu}{\mu[\mu^2 r^2 - \mu_o^2 r_o^2 \sin^2 z_o]^{1/2}} \tag{4}$$

where $r_o = r_e + h_o$.

If the ray strikes an observer located on the earth's surface, we call its refraction angle the astronomical refraction. However, if the ray misses the earth and passes on through the atmosphere to a satellite observer, the

the total refraction is twice the astronomical refraction, R_o, which would be measured by an observer stationed at the point of ray tangency to the atmosphere. The subscript s will designate measurements made at the satellite. Then,

$$R_s = 2R_o \quad \text{with} \quad z_o = 90°$$

$$R_s = 2\mu_o(r_e+h_o)\int_1^{\mu_o} \frac{d\mu}{\mu[\mu^2(r_e+h)^2-\mu_o^2(r_e+h_o)^2]^{1/2}} \tag{5}$$

In Eq. (5) and subsequent equations the subscript o indicates values at the point of tangency.

Density and refractivity are connected by Dale and Gladstone's Law

$$\nu = k\rho = \mu - 1; \tag{6}$$

thus the connection between satellite refraction and the atmospheric density.

The literature contains a great deal of work on the calculation of the astronomical refraction angle, once a model atmosphere is prescribed. Of particular interest is the assumption of an isothermal atmosphere where the scale height, H, is defined by

$$H = \frac{R^*T}{Mg} \tag{7}$$

where

R^* = universal gas constant

T = temperature

M = mean molecular weight

g = acceleration of gravity

We may then write

$$\rho = \rho_o e^{(h_o-h)/H} \tag{8}$$

and by substitution in (5) with change of variable

$$R_s = 2\mu_o(\mu_o-1) \int_{h_o}^{\infty} \left(\frac{r}{H}\right) \frac{e^{(h_o-h)/H}\, dh}{\mu[(r_e+h)^2\mu^2-r^2\mu_o^2]^{1/2}} \tag{9}$$

which with certain approximations can be manipulated to obtain the classical formula[1]

$$R_o = k\rho_o \sqrt{\frac{\pi r_o}{2H}} \tag{10}$$

Model atmospheres other than isothermal have likewise been utilized, with results considerably more complicated than (10).

The inverse problem, that of specifying the atmosphere from a knowledge of refraction, has not been treated extensively.

B. SOLUTION OF THE INVERSE PROBLEM

Specification of the density profile of the real atmosphere from a knowledge of one refraction angle is patently impossible. However, the satellite will make many observations at various levels during occultation so that a continuous function is provided:

$$R_s = R_s(h_o)$$

The $R_s(h_o)$ data enables one to solve the inverse problem of recovering an atmospheric density profile. This principle may be demonstrated by considering Eq. (11), which is derived from Eq. (5) by dropping certain higher order terms.

$$R_s(h_o) = \sqrt{2r_o}\, k \int_{h_o}^{\infty} \frac{d\rho}{dh} \frac{dh}{\sqrt{h-h_o}} \tag{11}$$

Equation (11) is quite general in that it incorporates an arbitrary density profile; it is an integral equation similar to Abel's Integral Equation, and has the solution

$$\rho(h) = -\frac{1}{\pi\sqrt{2r_o}\, k} \int_{h}^{\infty} \frac{R_s(h_o)\, dh_o}{\sqrt{h_o-h}} \tag{12}$$

This solution can be verified by substitution of (12) into (11) with h_o replaced by x as the variable of integration:

$$R_S = -\frac{1}{\pi}\int_{h_o}^{\infty}\frac{dh}{\sqrt{h-h_o}}\frac{d}{dh}\int_{h}^{\infty}\frac{R_S(x)\,dx}{\sqrt{x-h}} \tag{13}$$

Deriving the differential

$$\frac{d}{dh}\int_{h}^{\infty}\frac{R_S(x)\,dx}{\sqrt{x-h}} = \lim_{\epsilon\to 0}\frac{1}{\epsilon}\left[\int_{h+\epsilon}^{\infty}\frac{R_S(x)\,dx}{\sqrt{x-(h+\epsilon)}} - \int_{h}^{\infty}\frac{R_S(x)\,dx}{\sqrt{x-h}}\right] \tag{14}$$

The variable of integration of the first integral on the right-hand side is now changed, $x \to x+\epsilon$, and we have

$$\frac{d}{dh}\int_{h}^{\infty}\frac{R_S(x)\,dx}{\sqrt{x-h}} = \lim_{\epsilon\to 0}\frac{1}{\epsilon}\int_{h}^{\infty}\left[R_S(x+\epsilon) - R_S(x)\right]\frac{dx}{\sqrt{x-h}} = \int_{h}^{\infty}\frac{dR_S}{dx}\frac{dx}{\sqrt{x-h}} \tag{15}$$

When (15) is substituted into (13)

$$R_S = -\frac{1}{\pi}\int_{h_o}^{\infty}\frac{dh}{\sqrt{h-h_o}}\int_{h}^{\infty}\frac{dR_S}{dx}\frac{dx}{\sqrt{x-h}} \tag{16}$$

This integral can be solved by inverting the order of integration as follows:

$$R_S = -\frac{1}{\pi}\int_{h_o}^{\infty}\frac{dR_S}{dx}\,dx\int_{h_o}^{x}\frac{dh}{\sqrt{(h-h_o)(x-h)}} \tag{17}$$

But

$$\int_{h_o}^{x}\frac{dh}{\sqrt{(h-h_o)(x-h)}} = -2\tan^{-1}\sqrt{\frac{x-h}{h-h_o}}\Bigg]_{h_o}^{x} = \pi \tag{18}$$

Therefore (17) becomes

$$R_S(h_o) = -\int_{h_o}^{\infty} \frac{dR_S}{dx}\,dx = -R_S\Big]_{h_o}^{\infty} = R_S(h_o) \qquad (19)$$

If the star is acquired by the sensor at a high altitude where the refraction is vanishingly small, and is tracked downward to occultation where refraction is a maximum, the scan will provide refraction angle as a function of time. Knowledge of the satellite's position and that of the star, together with a correction for the deflection of the ray, will provide h_o as a function of time. Thus $R_S(h_o)$ is available for use in Eq. (12) to compute the density, $\rho(h)$. The two assumptions involved in Eq. (11) and the derivation of $h_o(t)$ are discussed at length in Sections II-C and II-D.

Once the density profile is obtained, it may be integrated to yield a pressure profile. Since the initial pressure is a boundary condition it must be estimated, but the error due to this estimate is reduced by an order of magnitude after 13 km of integration. The integration may be started above the level for which "accurate" density data are claimed so that comparable accuracies will be obtained for pressures about 5 km below densities. Temperature may be deduced from the pressure and density.

For example, a constant error in absolute density of ±5% at 25 km is equivalent to ±18% at 33 km and ±2.3% at 20 km. If integration were begun at 33 km, at 20 km the pressure would be in error less than ±5% due to density inaccuracy. The initial pressure at 33 km would have to be estimated and might be off 15%, adding only 1.5% error in pressure at 20 km. Thus comparable errors of about 5% would obtain in pressure (and temperature) at 20 km and density at 25 km.

C. EFFECT OF TWO APPROXIMATIONS

1. Non-Sphericity*

The ability to use the refraction of starlight as an atmosphere's density probe depends critically upon the ability to reproduce mathematically the refractivity of the atmosphere from a discrete set of refraction angle measurements. It has been shown previously that for a spherically stratified exponential atmosphere this inversion is elementary. However, the real atmosphere is not spherically stratified; thus one must consider this effect very carefully. Fortunately, the lateral variations of density (i.e., refractivity) are small compared to the vertical changes, permitting a linear analysis of

*This analysis is due to Mr. Paul B. Hays.

the phenomenon. Thus one may proceed to study this added problem iteratively, as was done previously.

Rewriting the basic refraction equation (1)

$$\frac{d\vec{T}}{ds} = \frac{1}{\mu}\vec{T}x(\vec{Grad}\ \mu x\vec{T}) \tag{20}$$

In this equation $\vec{T}$ represents a unit vector tangent to the ray.

This differential equation must be integrated from the star to the satellite in order to obtain the total refraction at the satellite. This may be written formally as follows:

$$\vec{R} = \vec{T}_S = \vec{T}_{-\infty} = \oint_{s_{-\infty}}^{s_S} \frac{1}{\mu(s)}\vec{T}(s)\ x[\vec{Grad}\ \mu(s)x\vec{T}(s)]ds \tag{21}$$

where subscript s refers to the satellite and subscript $-\infty$ represents some position on the far side of the atmosphere where there is no refraction. To simplify this solution an iterative method is applied which assumes as a zeroth iterative the unrefracted ray. That is, since the refraction is small, the error in following a straight ray will be very small. The only problem remaining is to write the integrand of (21) in such a form that the integrals can be evaluated. The coordinate system shown in Fig. 1 is introduced, where $s^{(0)}$ is the line $y = r_e+h_o$, $z = 0$, $x = s$ and $s_\theta = rd\theta$.

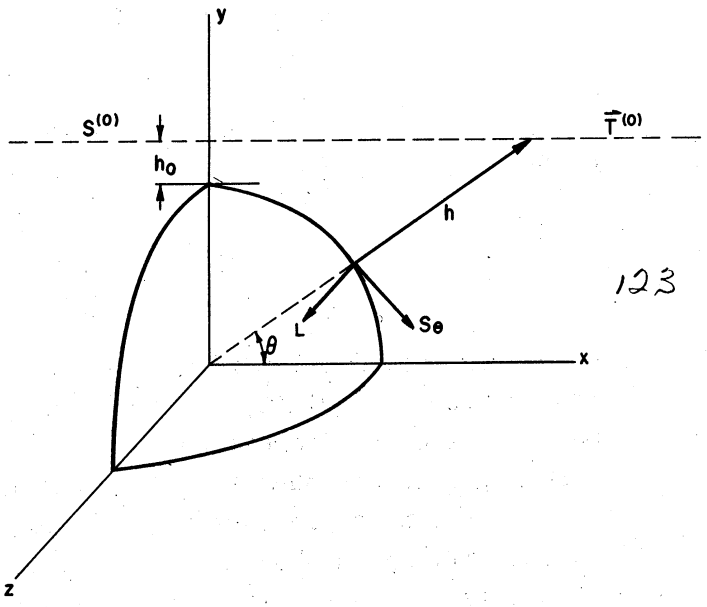

Fig. 1. Coordinates employed in non-sphericity analysis.

In this system:

$$\frac{d\vec{T}(1)}{dx} = \frac{1}{\mu}\left(\frac{\partial\mu}{\partial h}\sin\theta\vec{i}_y + \frac{\partial\mu}{\partial s_\theta}\cos\theta\vec{i}_y + \frac{\partial\mu}{\partial L}\vec{i}_z\right) \tag{22}$$

In order to simplify still further, introduce the small angle assumptions on $\vec{T}(1)$, so that

$$\vec{T}(1) = \vec{i}_x + R_P\vec{i}_y + R_L\vec{i}_z$$

where R_P = refraction angle in the plane x, y; and R_L = refraction angle out of this plane.

Thus:

$$R_P = \int_{-\infty}^{\infty}\frac{1}{\mu}\left(\frac{\partial\mu}{\partial h}\sin\theta + \frac{\partial\mu}{\partial s_\theta}\cos\theta\right)dx \tag{23}$$

and

$$R_L = \int_{-\infty}^{\infty}\frac{1}{\mu}\frac{\partial\mu}{\partial L}\,dx \tag{24}$$

Now introduce Dale and Gladstone's Law [Eq. (6)] and neglect the square of $k\rho$ compared to 1:

$$R_P \cong k\int_{-\infty}^{\infty}\left(\frac{\partial\rho}{\partial h}\sin\theta + \frac{\partial\rho}{\partial s_\theta}\cos\theta\right)dx \tag{25}$$

and

$$R_L = k\int_{-\infty}^{\infty}\frac{\partial\rho}{\partial L}\,dx \tag{26}$$

At this point the problem is completely formulated, and one need only introduce a correct form for $\rho(x,y,z)$. This is done by introducing a pseudo-exponential atmosphere with variable mean density and scale height:

$$\rho = \rho_o(s_\theta z)e^{-(h-h_o)/H(s_\theta, z)} \tag{27}$$

Then:

$$\frac{\partial \rho}{\partial h} = -\frac{\rho_o(s_\theta, L)}{H(s_\theta, L)} e^{-(h-h_o)/H(s_\theta, L)} \tag{28}$$

$$\frac{\partial \rho}{\partial s_\theta} = \frac{\partial \rho_o(s_\theta, L)}{\partial s_\theta} e^{-(h-h_o)/H(s_\theta, L)} + \rho_o(s_\theta, L)\left[\frac{h-h_o}{H^2(s_\theta, L)} \frac{\partial H(s_\theta, L)}{\partial s_\theta}\right] e^{-(h-h_o)/H(s_\theta, L)} \tag{29}$$

$$\frac{\partial \rho}{\partial L} = \frac{\partial \rho_o}{\partial L}(s_\theta, L) e^{-(h-h_o)/H(s_\theta, L)} + \rho_o(s_\theta, L)\left[\frac{h-h_o}{H^2(s_\theta, L)} \frac{\partial H(s_\theta, L)}{\partial L}\right] e^{-(h-h_o)/\mu(s_\theta, L)} \tag{30}$$

Now introducing the parabolic approximations for θ, $h-h_o$, and s_θ in terms of x, one finds that

$$s_\theta \cong x, \quad h-h_o \cong \frac{x^2}{2(r_e+h_o)}, \quad \sin\theta \cong 1, \quad \cos\theta \cong \frac{x}{r_e+h_o} \tag{31}$$

Then:

$$R_P = -k \int_{-\infty}^{\infty} \left\{ \frac{\rho_o(x,i)}{H(x,L)} \left[1 + \frac{\partial H(x,L)}{\partial x} \frac{x^3}{2H(x,L)(r_e+h_o)^2}\right] + \frac{\partial \rho_o(x,L)}{\partial x} \frac{x}{r_e+h_o} \right\} e^{-\frac{x^2}{2(r_e+h_o)H(x,L)}} \tag{32}$$

$$R_L = k \int_{-\infty}^{\infty} \left\{ \frac{\partial \rho_o(x,L)}{\partial L} + \frac{\rho_o(x,L)}{H^2(x,L)} \frac{\partial H(x,L)}{\partial L} - \frac{x^2}{2(r_e+h_o)} \right\} e^{-\frac{x^2}{2(r_e+h_o)H(x,L)}} \tag{33}$$

The mean density and scale height are then expanded along the line x in a Taylor series, i.e.,

$$\rho_o = \bar{\rho}_o + \bar{\rho}_o\rho'(0)x + \bar{\rho}_o\rho''(0)x^2/2 + \bar{\rho}_o\rho'''(0)x^3/3 + \ldots + \bar{\rho}_o\rho_L(0)L + \bar{\rho}_o\rho_L'(0)x + \bar{\rho}_o\rho_L''(0)x^2/2 + \ldots \tag{34}$$

where

$$\rho'(0) = \frac{1}{\bar{\rho}_o} \left.\frac{\partial \rho}{\partial x}\right|_{\text{at } x = 0} \tag{35}$$

$$\rho_L(0) = \frac{1}{\bar{\rho}_o} \left.\frac{\partial \rho}{\partial L}\right|_{\text{at } x = 0} \tag{36}$$

and similarly for H.

These derivatives are the density variations noted at the point of closest approach of the unrefracted ray. They are now substituted into the approximate refraction formulas above and the formulas are integrated, resulting in the following expressions for the refraction angles:

$$R_P = R_{P_o} \left\{ 1 + \frac{H_o}{2} (r_e + h_o) \left[\rho''(0) + \frac{H''(0)}{2} + H'(0)\rho'(0) - 3H'(0)^2 \right] + \ldots \right. \tag{37}$$

$$R_L = - R_{P_o} H_o \left[\rho_L(0) + \frac{H_L(0)}{2} \right] \tag{38}$$

where

$$R_{P_o} = -k\rho_o \sqrt{\frac{2\pi(r_e + h_o)}{H_o}} \tag{39}$$

is the refraction for a spherically stratified atmosphere as in Eq. (10).

In order to clarify the significance of the additional terms, Table I has been included to indicate the effects of extreme atmospheric gradients.

Table I was constructed by scanning meteorological records for extreme gradients, computing the derivatives, and substituting in Eqs. (37) and (38). The importance of the results is threefold. First, it proves the nearly negligible character of the spherical stratification assumption in the development of the general refraction equations. Second, it proves the negligible error inherent in assigning the refraction-density to the geographical position of ray tangency. Third, it proves the entirely negligible character of refraction in the lateral plane.

TABLE I

EFFECTS OF EXTREME ATMOSPHERIC GRADIENTS

Extreme Case of Non-Spherical Stratification	R_P/R_{P_o}	R_L/R_{P_o}
Strong extratropical gradient of P and T (300 mb)	1 + .006	- .001
Intense cold trough (300 mb)	1 + .008	
Strong hurricane (500 mb)	1 + .026	- .002
Surface frontal zone (1000 mb)	1 + .013	

2. Effect of Integrating Along Straight Rather Than Refracted Ray

In order to obtain the solution for the inversion, Eq. (11) was written on the basis of the geometry of an unrefracted ray. Likewise, the manipulation required in passing from Eq. (9) to Eq. (10) involves the approximations $\mu \cong \mu_o \cong 1$ and $\sqrt{2r+h-h_o} \cong \sqrt{2r}$ in the denominator of the integrand, which corresponds again to integration along a straight ray path.

To determine the significance of this approximation, the following approach was taken.

Equation (9), the exact expression for refraction in an isothermal atmosphere, was evaluated by graphical methods.

Equation (9), after application of the approximations, becomes

$$R_S = 2(\mu_o - 1) \int_{h_o}^{\infty} \frac{(\sqrt{r_o/2})}{H} \frac{e^{(h_o-h)/H} dh}{\sqrt{h-h_o}} \qquad (40)$$

and this expression was evaluated by both analytic and graphical methods.

The evaluations were carried out for a ray tangent at the earth's surface, since this ray's departure from a straight line is greatest. The scale height was 7.5 km and $\mu_o = 1.000277$.

Upon graphic evaluation, Eq. (9), the exact expression, yielded R_S = 75.48 minutes, while Eq. (40) yielded R_S = 68.76 minutes. Equation (40), evaluated analytically, gave R_S = 69.44 minutes.

Thus, we conclude from the close agreement (1%) between graphical and analytic results for Eq. (40) that the graphical technique is accurate. Knowing this, we further conclude that the comparison between graphical evaluations is valid and that the approximations are seen to be not at all negligible, but equal to 9% at the earth's surface.

Clearly, integrating along a straight rather than refracted ray will introduce significant errors. Effort is being directed toward an analytic solution of integration along the refracted ray. The present estimate, however, is that a solution by numerical methods will be required. With the availability of high-speed computers, a numerical method should not be considered undesirable nor necessarily less ideal than an analytic solution for this problem.

D. LOCATION OF TANGENT POINT

Simple geometry is employed to obtain the geographical position of ray tangency, and is shown in Fig. 2.

The satellite's position is assumed known, as well as the refraction angle and direction of the star. Referring to Fig. 2, lines SS' and SB can be drawn with the given information. The normal to SB is drawn through the earth's center, determining P and the normal distance p. Knowing p, OP' can be drawn normal to the star's direction, determining BB' and hence the intersection B. The geographical position of B, GP, yields latitude and longitude. Appendix A contains a complete discussion of the determination of latitude and longitude.

Less simple and more important is the determination of the ray's height, h_o, at tangency. The radius $OB = r_e+h_o+b$ is known. Thus, the determination of b is equivalent to the determination of h_o.

A direct result of Snell's Law of refraction is that for any ray path in a continuous, spherically stratified atmosphere

$$r\mu \sin z = \text{constant} \tag{41}$$

where, of course, z is measured from the perpendicular to the gradient of μ.

Thus, in Fig. 2,

$$r_s\mu_s \sin z_s = r_o\mu_o \sin z_o \tag{42}$$

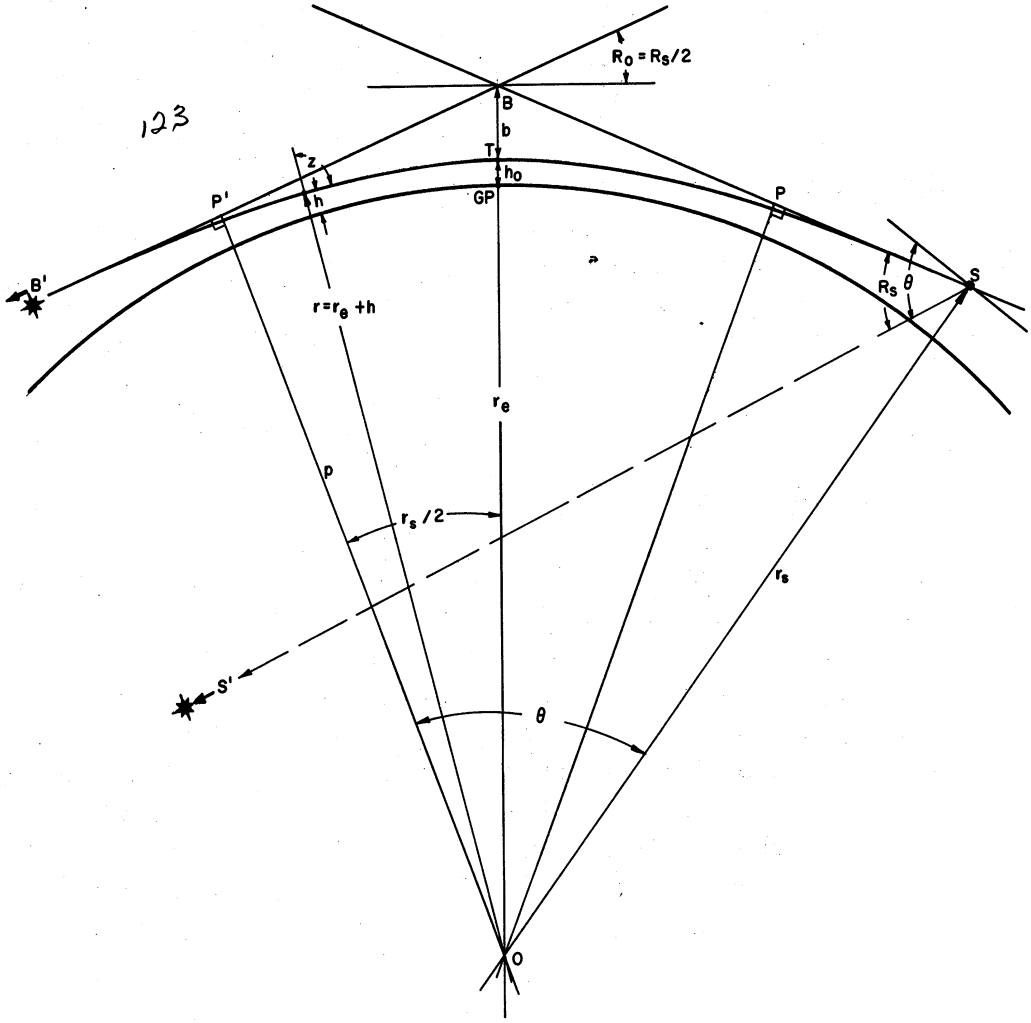

Fig. 2. Geometry of refraction.

and in triangle OBS

$$\frac{\sin z_S}{\sin z_B} = \frac{r_e+h_o+b}{r_S} \tag{43}$$

But since $\mu_S = 1$ and $\sin z_o = 1$,

$$r_o\mu_o = (r_e+h_o+b)\sin z_B \tag{44}$$

However,

$$\sin z_B = \sin(90°+R_o) = \cos R_o ,$$

and

$$b = \frac{(r_e+h_o)\mu_o}{\cos R_o} - (r_e+h_o) \tag{45}$$

or

$$b = (r_e+h_o+b)\left(1 - \frac{\cos R_o}{\mu_o}\right) \tag{46}$$

Equation (46) is exact with only the assumption of spherical stratification. Departures from spherical stratification apparently have a negligible effect on the determination of b. This may be concluded from the analysis in Section II-C-1. The distance b, and consequently h_o, is a function of R_o and μ_o only, and independent of the ray path or density distribution along the ray.

It can be shown that about 99% of the refraction of a ray tangent at h_o occurs within h_o+25 km of the surface. Using temperature extremes of the real atmosphere which may exist up to 50 km, and considering limiting isothermal cases where H = 6.4 and 8.4 km, the limit of variation in μ_o, and thus in b, may be computed from Eq. (10).

The result is a maximum index of refraction change of ±.0015%. Equation (46) then shows b to have a maximum error of 90 m.

A 90-meter altitude error is equivalent to about 1.1% error in ρ_o or about 1.1% in R_S. In any inversion formula used to retrieve the density function, such as Eq. (12), the integral of $R_S(h_o)$ from h to ∞ will no doubt appear. Since the maximum error in the function $R_S(h_o)$ is a constant percentage,

the percentage error in the integral can be no more than this. In fact, if the errors in $R_s(h_o)$ should be at all scattered, the error in the integral will be considerably smaller. In view of these considerations, one would expect a maximum of 1% density error due to uncertainties in h_o, and these would be subject to an iterative improvement if necessary.

The foregoing applies to determination of longitude, latitude, and height of the point of tangency for a particular ray. During one scan, the tangent point moves downward and in the direction of satellite motion due to satellite motion, toward the satellite due to refraction, and westerly due to the earth's rotation.

Using the direction opposite to the satellite velocity vector as a reference, one may speak of the azimuth angle of a ray as the angle in the horizontal plane between the projection of the ray onto the plane and the reference. The altitude is the angle between the ray and the horizontal plane. Referring to Fig. 2, $R_s-\theta$ is the altitude, and if ω_p = satellite's angular velocity component in the OSB plane, $\theta = \omega_p t$ and $\theta = 90+R_s-\sin^{-1}[(r_e+h_o+b/r_s)\cdot\cos(R_s/2)]$.

R_s as a function of θ is shown in Fig. 3, while in Fig. 4 the time to occult is shown as a function of azimuth, Az, and tangent ray height, h_o. From Fig. 4 it may be noted that at 0° azimuth the time for the scan to move from h_o = 35 km to h_o = 5 km is 24 seconds, whereas at 30° azimuth the time is 28 seconds. At greater azimuths a proportionally greater time penalty is paid, so that at 45° the same scan requires almost 40 seconds.

The motion of the geographical position of the tangent point in the general direction of the satellite is shown in Fig. 5, where a non-rotating earth is assumed. $\hat{S}$ is the sub-satellite path and $\widehat{AA'}$ is the locus of geographical positions of light rays tangent to the atmosphere at 25-km height. $\widehat{BB'}$ is the locus of sub-satellite positions where 25-km rays would be seen by the satellite, and $\widehat{CC'}$ is the same for 5-km rays. Angle i is the inclination of the orbital plane to the normal to the direction of the star, which is the angle between planes determined by $\hat{S}$ and $\widehat{AA'}$. If the star is viewed directly aft of satellite, the geographical position moves from T to GP_2, which is 49.4 km, or 26!26 subtended at the earth's center, O.

From the spherical triangles in Fig. 5, we can write the path length $\overline{GP_1\ GP_2}$ of the scan's geographical position in going from 25- to 5-km height:

$$\overline{GP_1\ GP_2} = \cos^{-1}(\cos 26\text{!}26\ \cos \overline{TGP_1}) \qquad (47)$$

where

$$\overline{TX} = \sin^{-1}(\cot i \tan \theta_2)$$

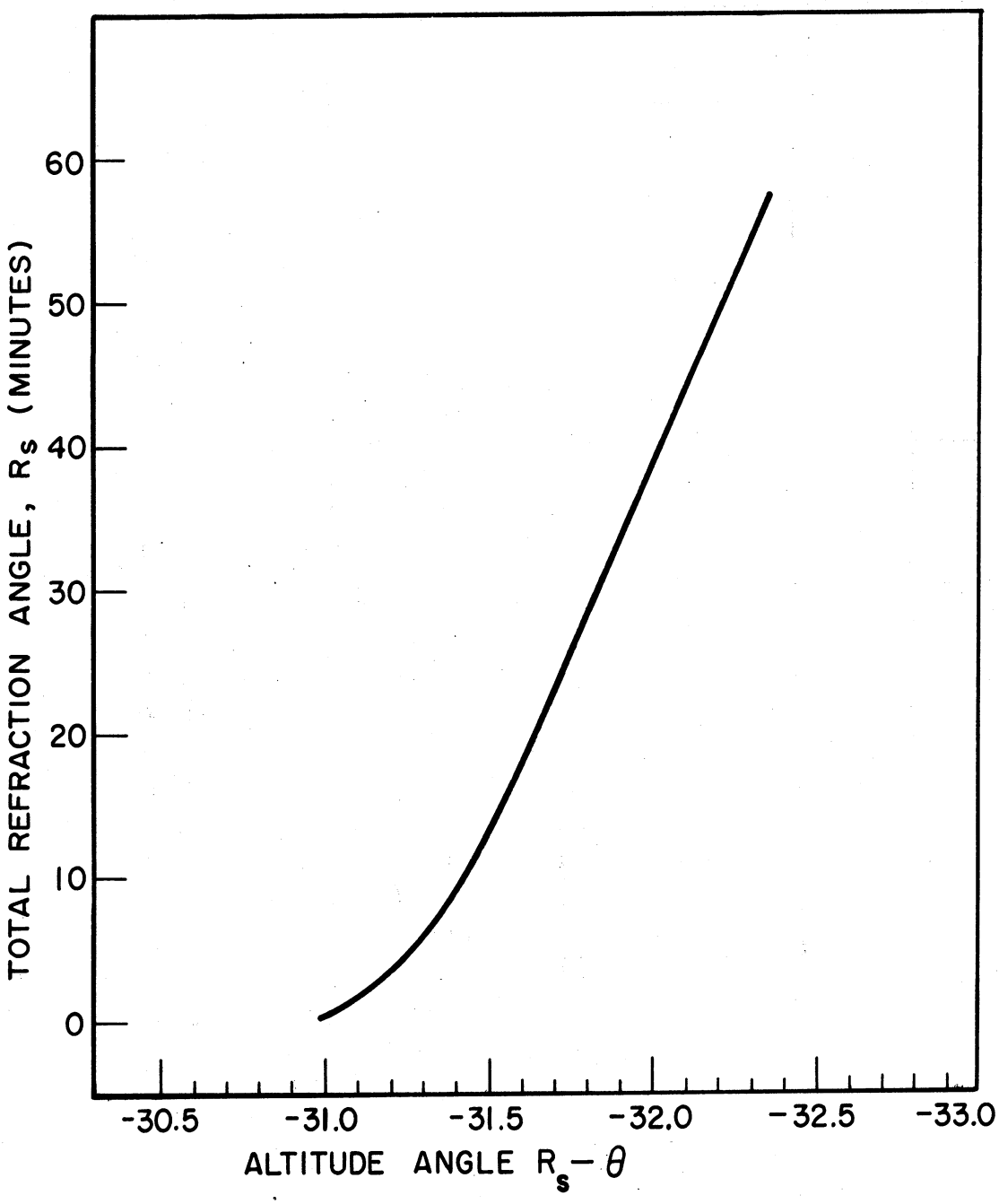

Fig. 3. Total refraction angle as a function of altitude angle.

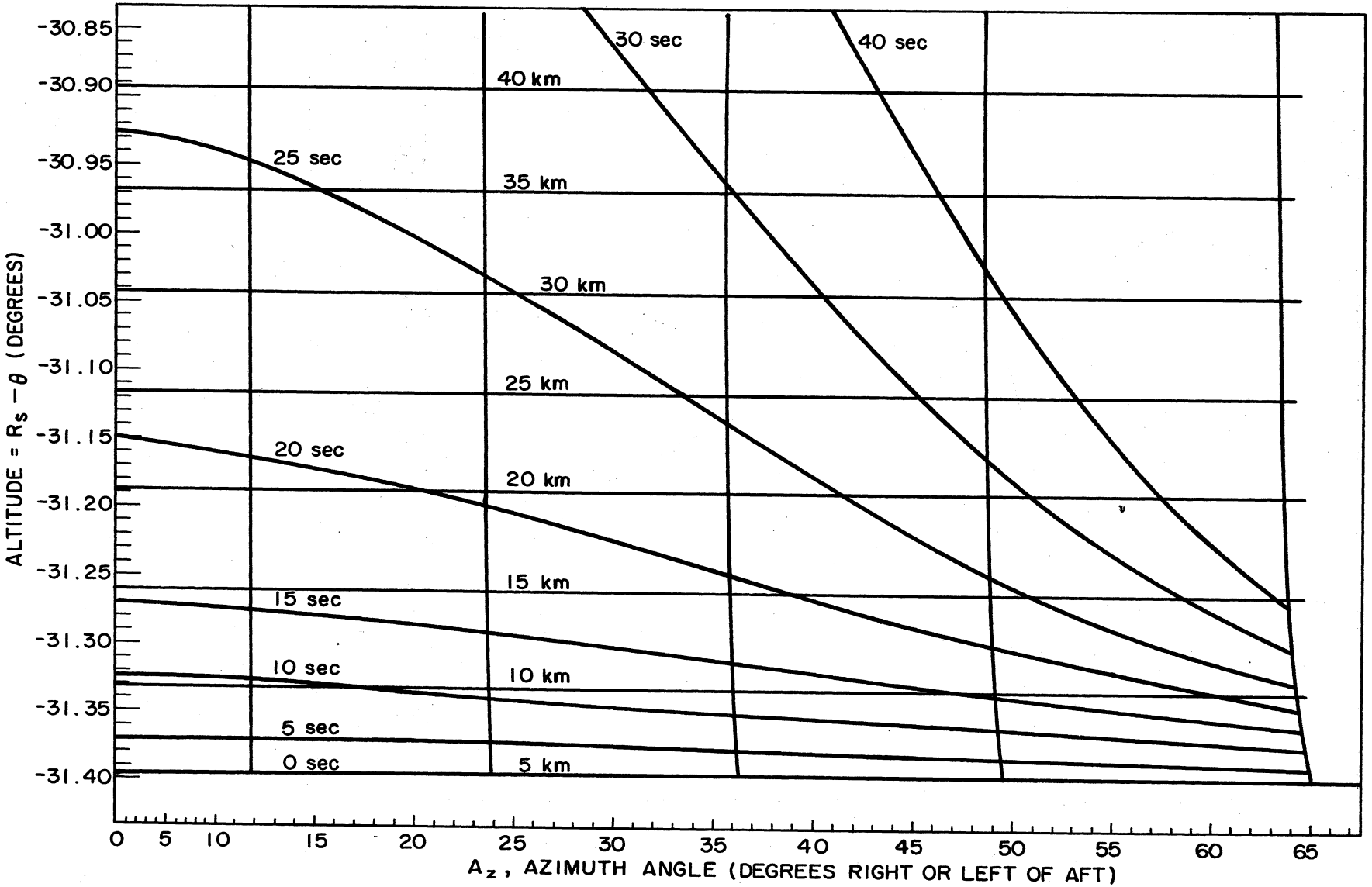

Fig. 4. Time to occult as a function of azimuth and tangent ray height.

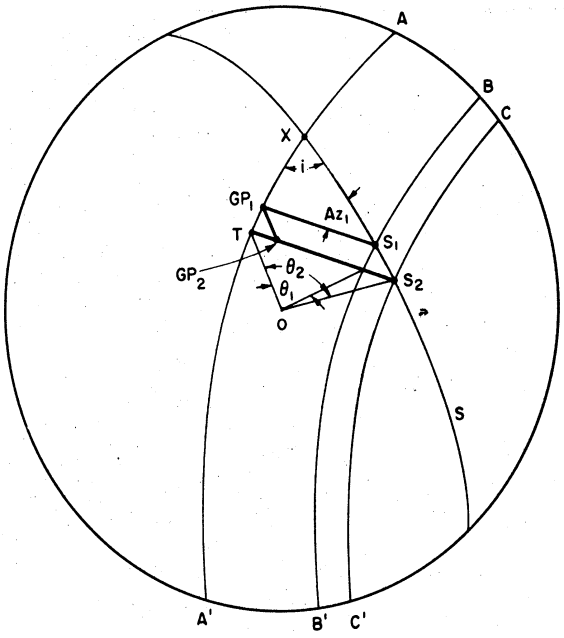

Fig. 5. Motion of geographical position of tangent point during a scan.

and

$$\overline{X\ GP_1} = \sin^{-1}(\cot i \tan \theta_1)$$

$$\text{azimuth} = \cos^{-1}(\sin i \cos \overline{TX}).$$

Scan length as a function of azimuth angle is shown in Fig. 6. These results are for a non-rotating earth. Scan time may be taken from Fig. 4 and rotation of the earth added vectorially.

E. MAGNITUDE OF REFRACTION

The angle measured, R_s, must have sufficient magnitude to be readily detected by the instrumentation. We may compute the approximate angles by Eq. (10), obtaining:

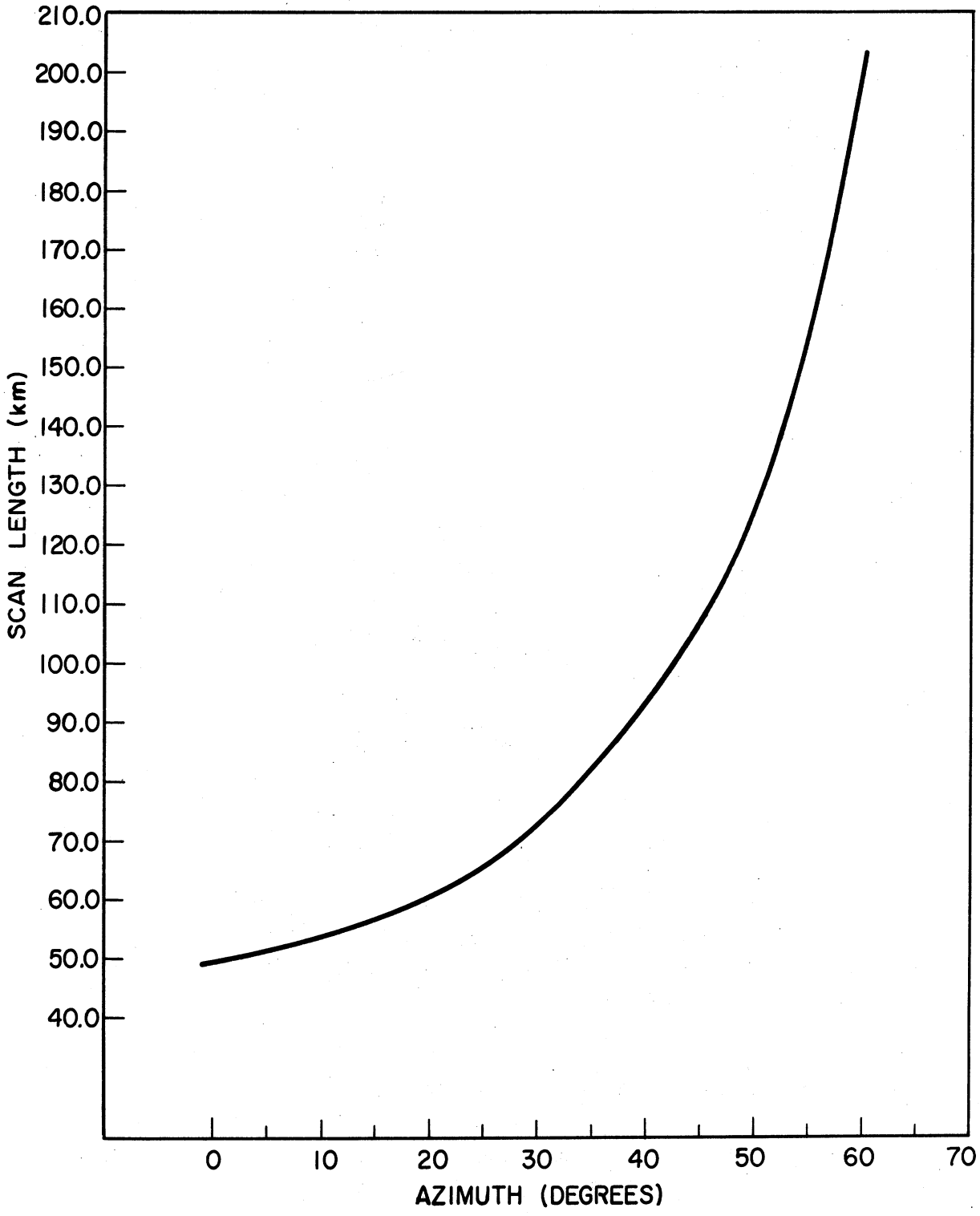

Fig. 6. Scan length as a function of azimuth angle.

TABLE II

APPROXIMATE ANGLES OF REFRACTION

h_o (km)	R_s (minutes)
0	69.4
5	41.7
10	23.4
15	11.0
20	5.0
25	2.3

F. SUMMARY

In summary, a single refraction scan consists of measuring the apparent position of a star relative to a space stabilized reference. While the light ray passes through little or no atmosphere and suffers no refraction, the star's angle with respect to the reference is known, is constant, and may be pre-computed. But if the star is viewed in a direction generally opposite to that of the satellite's velocity, the earth will appear to move upward and will eventually occult the star. Prior to occultation the starlight will pass through ever increasing atmosphere and be measurably refracted. This refraction will be sensed as an angular change relative to the space reference, and will be recorded in the satellite as a function of time. Probably, the star will be tracked from a tangent height of about 35 km downward to obscuration by clouds at roughly 5 km. The angles measured will vary from a few seconds to almost one degree, and the time involved will be a little less than one-half minute. Perhaps one angle per second would be recorded in digital form, together with a time reference, so that from 20 to 30 datum points would exist to reconstruct the function $R_s(t)$.

The function $R_s(t)$ would be reconstructed by ground based computers, which would compute $h_o(t)$, and thus $R_s(h_o)$ and $\rho(h)$. The density function would be integrated for pressure and temperature. The computation would include determination of the geographical position for each datum point. Tracking data would be an additional input required by the computers.

III. THE THEORETICAL BASIS FOR GLOBAL COVERAGE

A. TIME CONSIDERATIONS

The objective is to provide a density—temperature—pressure profile of the atmosphere from 5 to 25 km at as many locations on the earth's surface as are required by meteorologists for three-to-five day and longer range forecasts. Presently, adequate coverage exists only in North America and Europe. These data are derived from balloon-sondes, making an extension to polar, oceanic, and Communist-bloc areas all but impossible. A consensus of meteorological writers indicates that ρ-T-p profiles spaced 200 statute miles apart over the entire earth's surface would suffice for forecasting purposes.

Among the meteorological satellites, the Nimbus orbit most nearly approaches the ideal for refractive techniques. Therefore Nimbus orbital parameters have been used to determine the global coverage possible.

The Nimbus orbit is assumed to have these characteristics:

1. circular, height 1100 km, period 107 minutes;

2. inclination of orbital plane to equator 99.89°;

3. precession of orbital plane in same direction and at same rate as mean sun;

4. injection into orbit over the equator at local noon; and

5. launched southward from Pacific Missile Range.

Since this orbit is nearly polar, all areas of the earth may be scrutinized. However, if observations are equally spaced timewise, a tremendous concentration of observations near the poles are a consequence of the polar orbit. The main problem, then, is to obtain an adequate observation density near the equator.

The satellite will make between 13 and 14 complete orbits per day and the earth will rotate about 26° during an orbit, which is about 1800 statute miles at the equator. The satellite's latitude change is roughly 3° or 200 statute miles per minute, thus it is evident that 9 scans per minute in the equatorial regions would be required for optimal coverage. Since the scan time is a function of azimuth angle only and in no case can be reduced beyond 21 seconds, three or four separate star-tracking devices would be required. In the mid-latitudes, two star-trackers would suffice and in polar regions, one.

For purposes of planning a prototype experiment, a compromise on two star-trackers is adopted. This will yield less than optimal observation densities in the tropics, but will be adequate or more so everywhere else. If at some later time additional equatorial observations are required, the number of star-trackers might be increased.

As the satellite moves in its orbit, the star-trackers would preferably track successive stars on various azimuths since this will have the effect of spreading the observations uniformly over the earth. On the other hand, as the azimuth angle increases, the time required for a scan increases, and fewer observations are possible. Time versus azimuth is shown in Fig. 7. The maximum azimuth which provides the optimum of observation density and observation location uniformity is rather arbitrary but appears to be in the neighborhood of 30°. At that angle, the scan time required is only about 15% more than directly aft, at 0°, yet the location of the tangent point lies 1200 miles from the sub-satellite path.

For a more accurate determination of p and T the scan should be started in the neighborhood of 35 km (as explained in Section II-B). We may also assume an average azimuth of 15° and, from Fig. 4, determine the average scan time to be 25 seconds. It has been estimated on the basis of similar devices that the time for the tracker to slew and lock on to a star will be under 3 seconds. On the average, then, one scan per tracker will be made in slightly less than 28 seconds, or about 236 scans per tracker per orbit.

B. CELESTIAL CONSIDERATIONS

In the preceding discussion, two important factors were not taken into account: first, the restrictions on star-tracking caused by sunlight; and second, the availability of a star in the desired position and at the desired time.

As for the sunlight, it appears that with present state-of-the-art equipment, only a few of the very bright stars may be tracked under daylight illumination. Exactly what angle below the horizon the sun must attain before the luminosity of the atmosphere is decreased sufficiently for tracking is not known. The determination of this angle will be difficult and probably not well estimated until the star-sensing equipment is selected and tested. Even then the difficulty of testing an instrument above the atmosphere may preclude a firm answer prior to an orbital flight. In the absence of other information, one may assume that it is possible to conduct refraction scans in one-half of the orbit—in particular, the half-orbit in which the points of ray tangency lie in the earth's shadow.

Therefore each tracker can make only 118 scans per orbit.

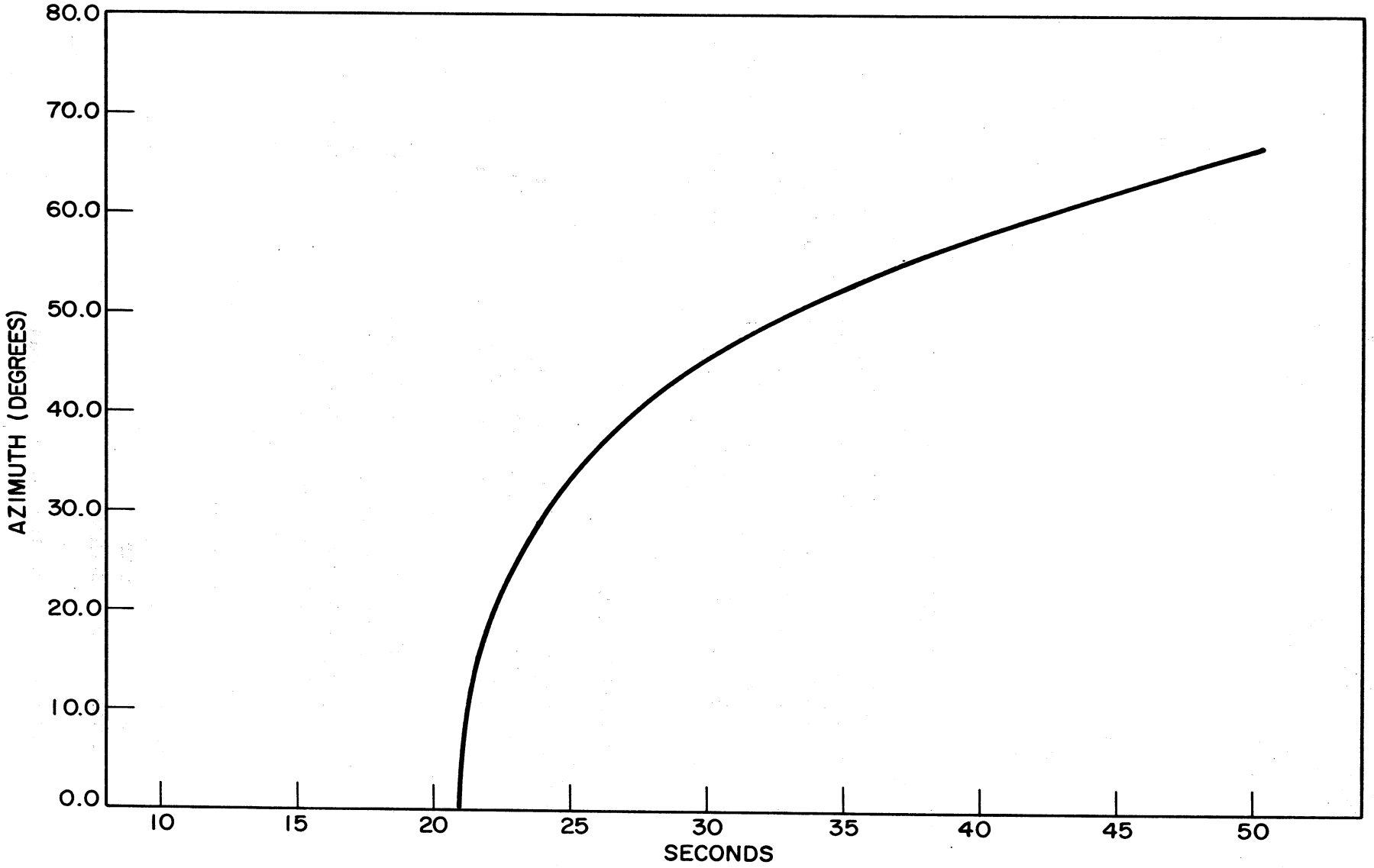

Fig. 7. Scan time vs. azimuth, Nimbus orbital parameters.

The number of possible scans per orbit has been based on the assumption that the tracker can slew and lock on to a star at about the 35-km level within 3 seconds. Regardless of the type of star-tracking equipment, it will be advantageous to track brighter stars, and we must deal with the questions of how bright an available star might be and what effect the launch date might have.

A 60° swath centered aft of the satellite would be swept out by the tracker's field of view. This constitutes one-half of the celestial sphere. Since the orbital plane is slowly precessing, the portion of the celestial sphere in view is constantly changing. Thus the launch date itself is of no consequence and for any given date a particular star field will be available.

To determine which stars would be available on any given day, the IBM 709 computer was utilized; an outline of its program is given here.

A magnetic-tape version of the Albany General (Boss) Catalog was obtained from Goddard Space Flight Center. This catalog has information on about 33,000 stars down to 7.5 magnitude, the stars ordered by right ascension. Since the primary purpose was to obtain the star-magnitude implications of various procedures, the stars were first sorted and counted by magnitude groups and a new tape made in which the stars remained ordered by right ascension within each magnitude group. The star count is shown in Fig. 8.

Next, the distribution of stars in each magnitude group by declination, north or south, and for each hour of right ascension was obtained. The results are shown in Table III.

It is well known that the star population is most dense around the galactic equator, or Milky Way. Another belt of stars, Gould's Belt of Bright Stars, is also of interest; it contains the nearer and brighter stars of what is known as the local cluster. The plane of Gould's Belt is inclined about 20° to the galactic plane. Both planes run approximately north-south. The galactic plane is inclined approximately 58° and Gould's Belt 65° to the equator. Since the orbit is inclined 80° to the equator it is evident that with the proper right ascension the bright stars would almost all be within the field of the star tracker, whereas three months later the orbit would intersect the belt sharply and the fewest bright stars would be seen.

The computer was programmed so that the inputs were the orbital elements and the desired star coordinates. The outputs were: geographical position of measurement, position of satellite at occultation, time of occultation, azimuth of star at occultation. The appropriate equations are given in Appendix A. This program was run for each two hours of right ascension or, equivalently, for each month of the year, for all magnitude groups less than 4.0.

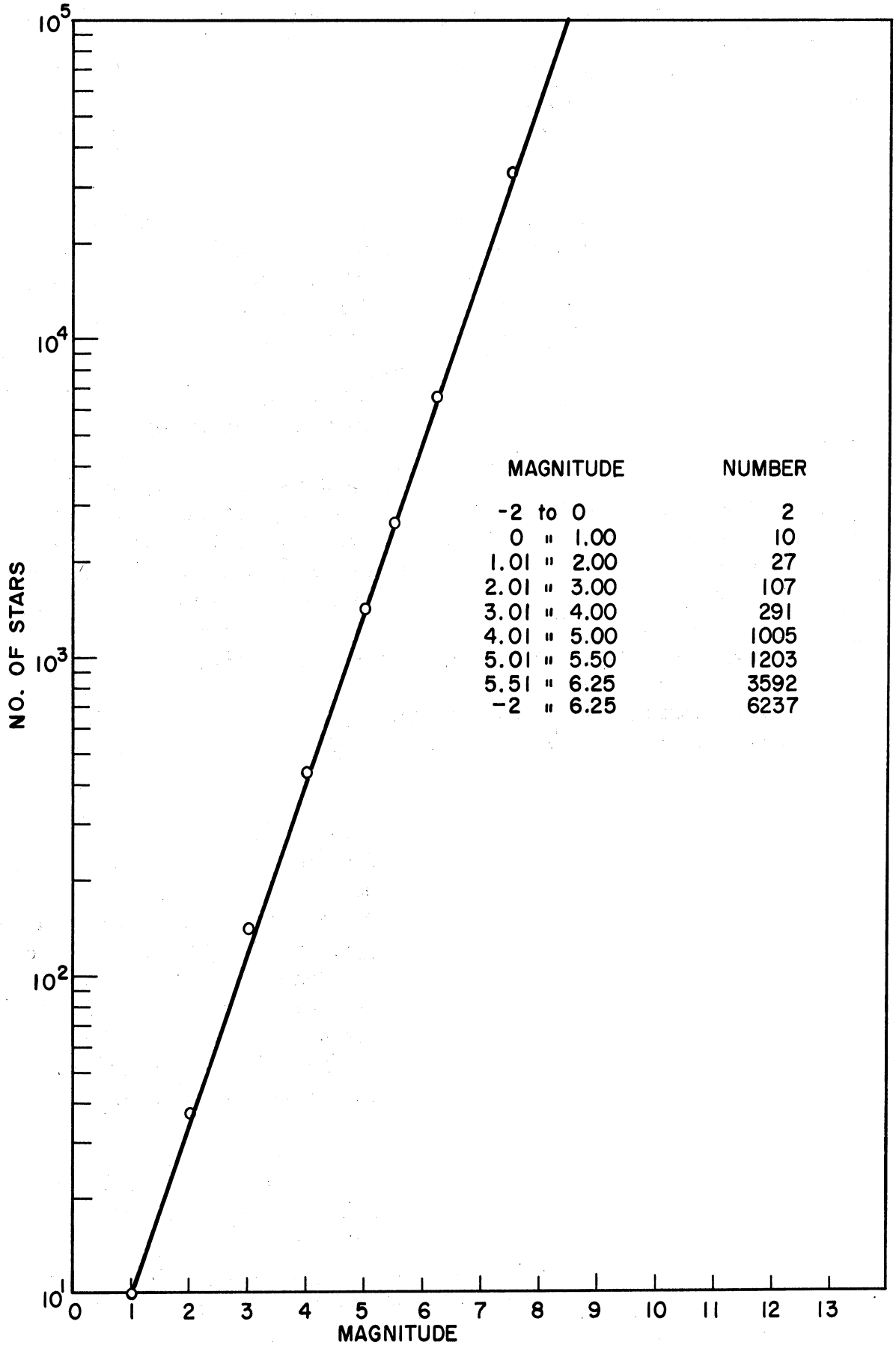

Fig. 8. Number of stars as a function of visual magnitude.

TABLE III

DISTRIBUTION OF STARS IN EACH MAGNITUDE GROUP

	Magnitude Group					
	<2.00	2.01-3.00	3.01-4.00	4.01-5.00	5.01-5.50	Total
Declination:						
North	18	47	141	458	584	1248
South	21	60	150	545	619	1395
Right Ascension: (Hours)						
0-1	0	7	7	30	37	81
1-2	1	4	13	34	41	93
2-3	0	3	6	36	47	92
3-4	1	3	16	44	39	103
4-5	1	1	15	50	62	129
5-6	6	11	15	57	63	152
6-7	5	1	10	44	74	134
7-8	4	2	14	50	79	149
8-9	1	4	10	47	58	120
9-10	1	4	14	44	49	112
10-11	1	3	14	37	41	96
11-12	1	3	10	29	48	91
12-13	4	9	10	35	49	107
13-14	2	4	7	37	33	83
14-15	3	8	9	41	37	98
15-16	0	6	20	48	52	126
16-17	2	7	15	47	49	120
17-18	1	10	20	35	37	103
18-19	2	4	11	46	68	131
19-20	1	2	15	43	68	129
20-21	1	3	13	43	49	109
21-22	0	3	9	35	39	86
22-23	1	3	14	49	43	110
23-24	0	2	4	44	41	91

The output of geographical positions was counted and sorted on the basis of:

1. azimuth of star < 30° when observed;

2. latitude of measurement in 10° groups from pole to pole; and

3. declination of star, north or south.

Only results from stars with azimuths < 30° were plotted. Results from northern and southern stars were separated in all cases because observations are restricted to northern stars when the satellite is injected southward on the equator at midnight, and are restricted to southern stars when injection is southward at noon. (This is approximate for two reasons: (1) it is a mere assumption that the portion of the orbit unused due to sunlight is exactly one-half; and (2) except at the equinoxes the dividing circle is not actually the celestial equator, but is inclined equally to the sun's declination.)

The use of southern stars increases the number of possible observations for any given magnitude by about 20%; therefore the noon-southward orbit is to be preferred.

The number of possible observations were plotted for each orbital plane according to latitude group and declination of star. Orbits were then classed as favorable on the bases of:

1. largest number of observations; and

2. highest proportion of observations in equatorial regions.

By the use of southern stars, it was determined that December 21 was the most favorable and August 21 the least favorable date. However, the star distribution in the various orbits was sufficiently uniform that even in the best orbital plane—that obtaining on December 21—only 153 observations per orbit were possible, when 236 were desired. (On August 21, only 88 were possible.) Thus, it was apparent that stars fainter than 4.0 would have to be used to approach the required density.

This process was repeated for the stars down to magnitude 5.5, for December 21 and August 21 dates. On the former date 812 southern stars, and on the latter date 647 southern stars were in the field. The data point positions of these stars are shown in Figs. 9 and 10 respectively. These stars were then subjected to hand selection of 236 stars from each orbit, spaced timewise so that they could all be scanned by two trackers and spaced geographically so that the best data point distribution could be attained. Stars were not divided north or south, but on the exact basis of the sun position on that date.

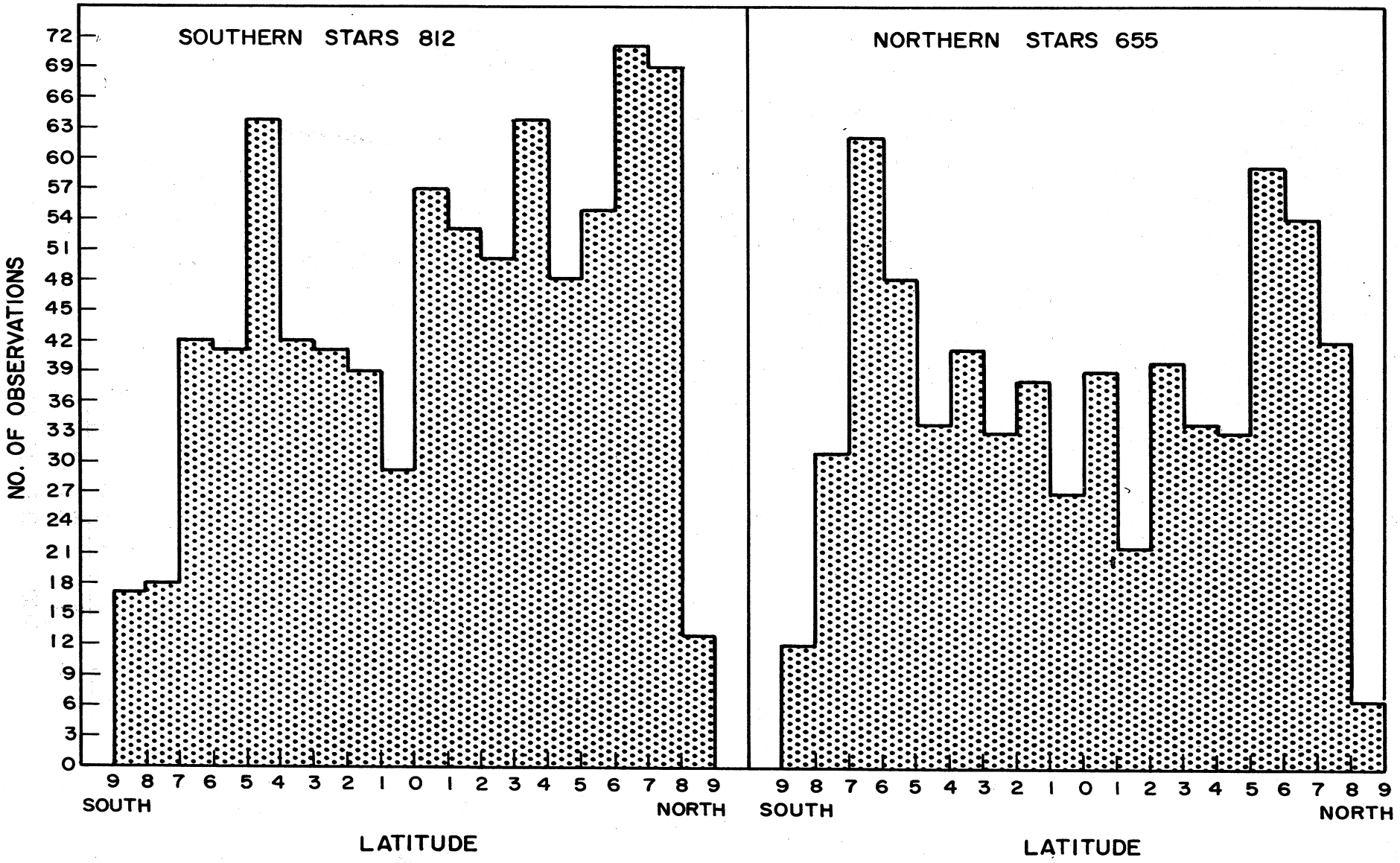

Fig. 9. Star data point positions, December 21.

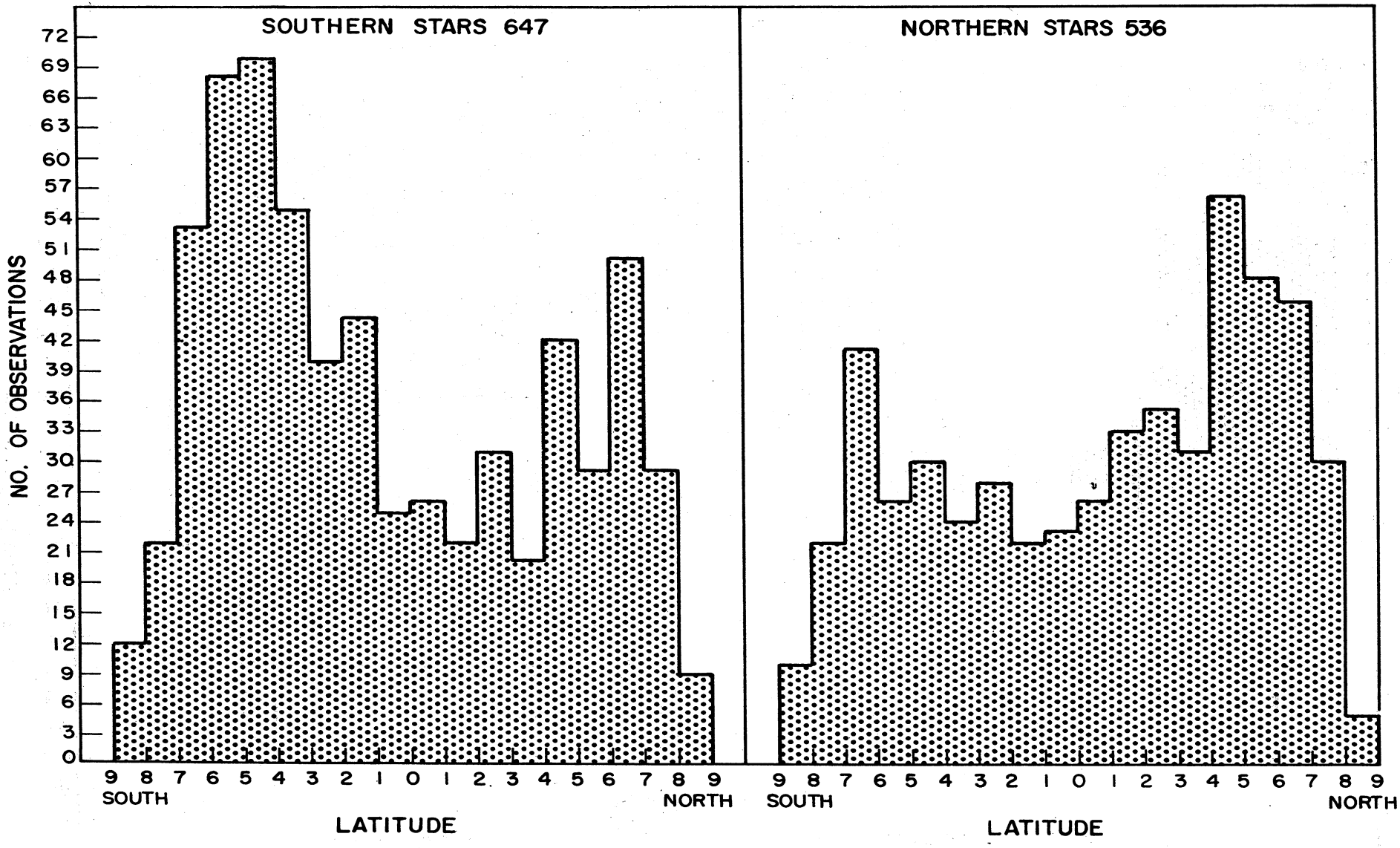

Fig. 10. Star data point positions, August 21.

The selected 236 stars were then fed into the computer and data points plotted for a 24-hour period on each of the two days. The results are shown in Figs. 11 and 12. Note that due to solar illumination, polar coverage in summer is impossible. Note also the tropical observation density obtained with two star-trackers.

The most significant conclusion of the star studies is that if stars brighter than magnitude 4.0 are used, the desired number of density scans can not be obtained on any date; whereas some magnitude brighter than 5.5 is sufficient for all orbits.

All work to date has been based on a noon-midnight orbit. Some Nimbuses might be flown in a sunrise-sunset or twilight orbit. It so, the star-trackers could be programmed to look away from the sun, in which case tracking on azimuths between, say, 15° and 60° would be possible. The consequence of higher azimuth angles is a longer scan and fewer scans per minute. Observations could be made for the entire orbit, however.

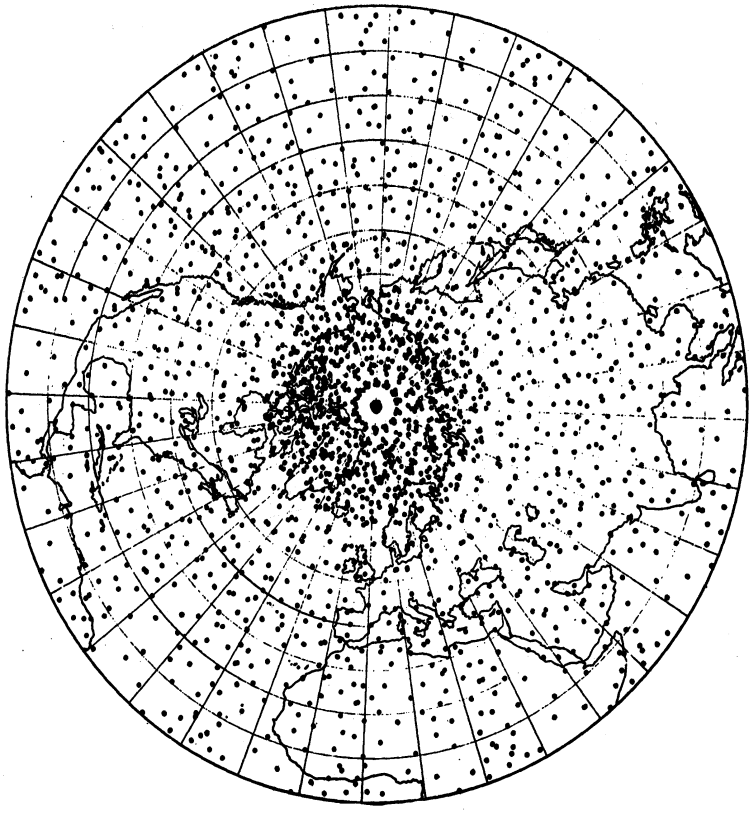

(a) Northern

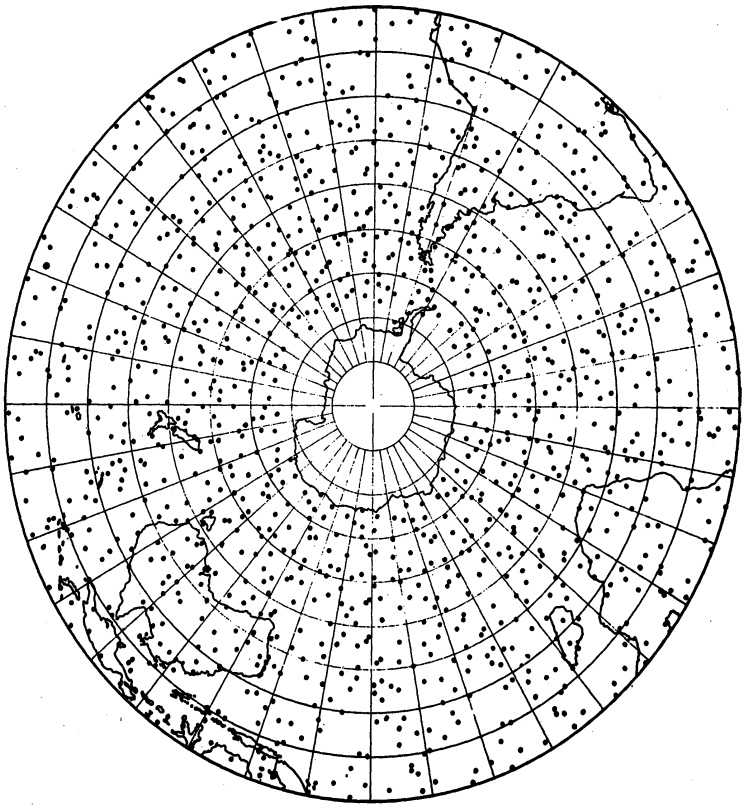

(b) Southern

Fig. 11. Plot of data point positions, December 21.

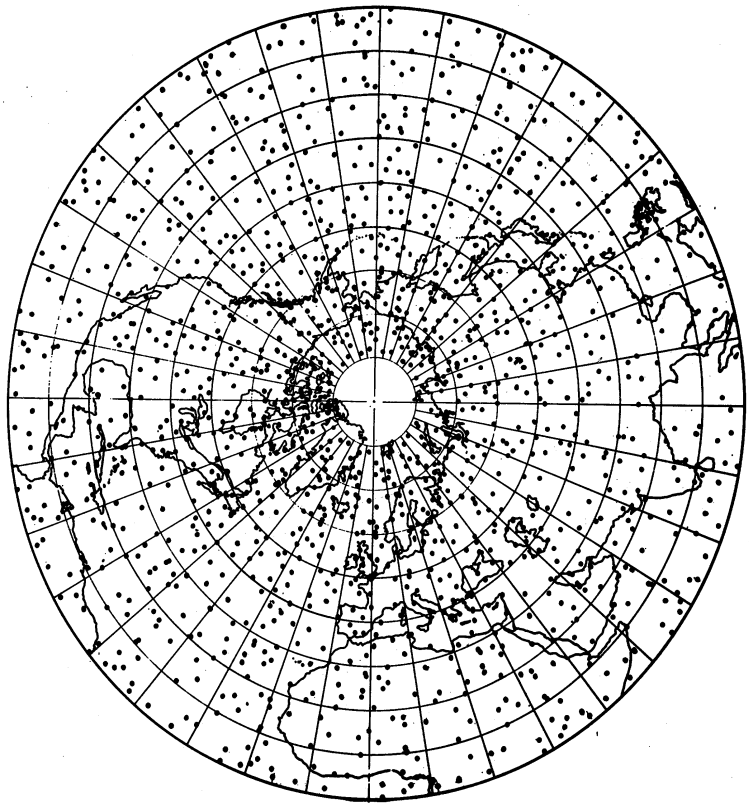

(a) Northern

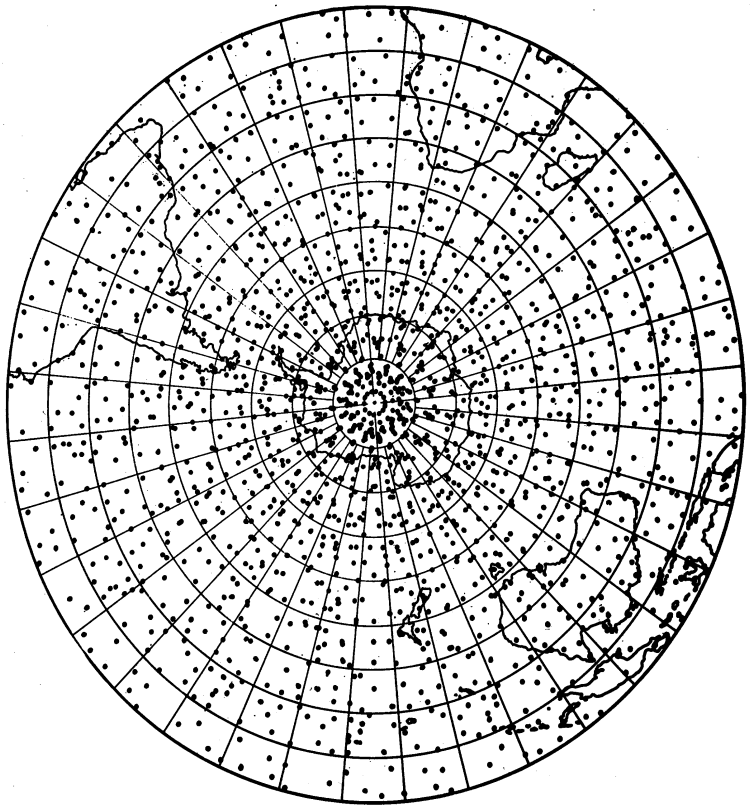

(b) Southern

Fig. 12. Plot of data point positions, August 21.

IV. PROPOSED EQUIPMENT AND METHODS

A. GENERAL

In the first report on this technique,[1] an attempt was made to describe the instrumentation which might be required. This description was little more than a guess and was included mainly to make the technique more lucid. Since that time significant changes in the "probable" type of equipment have taken place.

Again, the scheme proposed here is based more on conjecture than on equipment specifications, but includes the results of discussion with some of the leaders in the manufacture of star-tracking equipment.

The basis of the system is an automatic star-tracking telescope. For adequate global coverage (see Section III-A) two such telescopes are required, simply doubling the number of observations possible. The telescope (or at least a mirror) is attached to an inertial platform which is gyroscopically space-stabilized. The telescope is gimbal-mounted with digital, angular encoder-decoders and positioning apparatus. Associated with the telescopes are a clock accurate to a millisecond per orbit, two tape recorders, and programmer.

Prior to launch, the stable platform is aligned in a preferred orientation depending on launch time and orbital elements. After injection into circular orbit, it is expected that the rocket accelerations will have caused some error in the platform alignment. The first act of the programmer is to operate the tape recorder on which are stored a pre-programmed set of star coordinates for each tracker. The first stars observed by both trackers are high in the sky, unrefracted, and by far the brightest in their neighborhood. By use of an acquisition mode with wide field, the trackers lock on and the stable platform is then torqued to the desired alignment. (An alternate scheme is simply to measure the stable platform's orientation, and refer all future ground-based computations to its coordinates.) The star-trackers thus function as stellar monitors for the inertial system. The monitoring function can be repeated as often as necessary to correct for gyro drift while orbiting.

After the programmer is satisfied that the stable platform has been correctly oriented, it directs each telescope to the coordinates of the first star in its data-gathering program. The coordinates might be given to the nearest minute and the telescope could probably lock on in the tracking mode. During tracking, the star's angular changes along three gimbal axes would be recorded on magnetic tape, together with the time of one (the first, say)

measurement. Each successive measurement of angular change could be recorded at a precise time increment such as 1.000 second. After occultation or obscuration (persisting for some arbitrary length of time such as .5 seconds) the telescope would be commanded to slew to the next star in its recorded program, and the process would be repeated through the 118 stars in each telescope's program. The programmer would begin and end the measurements at the proper time relative to the sun.

The initial program of star coordinates could be recorded on a spacecraft tape recorder prior to launch. As the orbital plane precesses at about 1° per day, all stars remain with the same coordinates relative to the stable platform. However, the earth will gradually move out of this fixed telescope-star orientation and the field of stars, originally centered at 0° azimuth, will change azimuths at 1° per day, causing the center of the observations to lie off of the sub-satellite path and the occultations to take longer than desired. After a change of several degrees, it would be desirable to update the star programs; this would be done by the Command and Data Acquisition (CDA) station.

We shall now examine the information bits required for a new program. If we wished to identify the star among the 236 (which is not fundamentally required) 8 bits would be necessary. The direction can be resolved into two angles, one a maximum of 120° (azimuth), the other 180° (altitude). For one-minute accuracy we would need 1:7200 and 1:10,800 accuracies, or 13 and 14 bits respectively. The total required would thus be on the order of

$$236(8 + 13 + 14) = 8{,}260 \text{ bits.}$$

The simplicity of transmitting this information to the satellite would allow updating the program daily or oftener. Another possibility which might prove valuable is the ground selection of points of particular interest to be scanned. The ground computer would select appropriate stars which would yield measurements as close as possible to these points. Since the entire star program could be changed with only about 10,000 bits of information, a new program for each orbit might even be advantageous.

The data information rate must likewise be examined. As previously described, the measurements would require recording two angles to about one-second accuracy with neither angle exceeding 75 minutes. The accuracy is thus 1:4500 or 8 bits for each angle plus a bit to distinguish the axis, for a total of 17 bits per datum point. Additionally, each scan requires a time of one millisecond per orbit or 23 bits, and perhaps star identification with another 8 bits. The average scan is about 25 seconds, so we may assume 25 datum points per scan; consequently

$$(25 \times 17) + 23 + 8 = 456 \text{ bits per scan.}$$

Allowing for sync bits, etc., we might say the average scan would require recording 500 bits. At 236 scans per orbit the total information stored in an orbit would be only 118,000 bits. The telemetry system is capable of transmitting this information to the ground in a few seconds.

B. DATA PROCESSING

This information would be sent to the computer center from the CDA station by landline or radio link. The tracking data would likewise be sent to the computer center. Then the computer would reconstruct the geometry of each scan, determine the latitude and longitude of each datum point, and integrate to find $\rho(h)$, $T(h)$, and $p(h)$. These data would then be rapidly forwarded to the National Meteorological Center for meteorological analysis and dissemination.

Feedback at the NMC to the computer center might contain requests for additional coverage of certain areas. This input, together with an ephemeris for the next orbit, would enable the computer to choose a new set of stars. Their coordinates would be sent to the CDA station and relayed to the satellite on its next pass.

Obviously, the computers must handle the data from an orbit (and whatever new star commands are necessary) in an orbital period of 107 minutes, to prevent an impossible backlog of data. This means that a scan must be handled in 28 seconds, or that data processing must be done in the same amount of time as data acquisition.

Presently, the full program of computerized data reduction cannot be written because the final inversion formula, such as Eq. (12), is not known. Numerical methods are under test and results are expected soon. Preliminary results indicate it may be possible to avoid involved iteration; should this prove true, one IBM 7090 computer would probably be capable of reducing the data in real time.

Emphasis must be given to the relative simplicity of the data and command telemetry—on the order of 10^4 bits command and 10^5 bits readout per orbit. Yet this information has the capability of providing density, temperature, and pressure on a global basis.

C. TELESCOPE, CLOCK, TAPE RECORDER, AND TELEMETER

The telescope has been grossly described above. It must be mounted on a stable platform and be able to point over a hemispheric solid angle. Two telescopes, both mounted on the same stable platform, are likely to be used.

The importance of the stable platform is threefold: first, it provides a stable mount for the telescope, thus providing greater pointing and tracking accuracy; second, it provides a space reference which enables the telescopes to point quickly without search to any celestial coordinates chosen on the ground, thus saving power and time over a random search; and third, it provides a space reference against which to measure the refraction angle.

The telescope should have a tracking accuracy of ±6 arc seconds and a capability for tracking stars which appear as dim as the 10.5 magnitude. Some of the error implications of the tracking accuracy are discussed in Section VI. The star magnitude was arrived at on the following basis: from the work reported in Section III-B it was determined that stars of magnitude 5.0-5.5 would be the faintest required. However, since the telescope will be on a satellite looking through the entire earth's atmosphere, the attenuation in that medium must be accounted for. Appendix B is a complete discussion of this attenuation, the results of which are summarized thus:

1. Refraction causes a prismatic dispersion of the light flux and thus an attenuation.

2. Molecular (Rayleigh) scattering and Mie scattering (water vapor, haze, dust) also attenuate the light ray.

3. The attenuation due to refraction and molecular scattering is predictable and constant, whereas Mie scattering is variable. All are more severe nearer the earth.

4. At h_o = 5 km, the lowest measurements expected due to extinction by clouds, the refraction and molecular scattering will attenuate the light ray a total of 4 magnitudes. Mie scattering is estimated to cause about 1 magnitude more attenuation. At h_o = 10 km, the attenuation is 2.3 magnitudes, while at h_o = 25 km the attenuation is negligible.

The telescope should therefore be capable of tracking a star of the 10.5 magnitude. Since the magnitude required decreases sharply with altitude (at 10 km-7.8 magnitude), and at low altitudes the refraction angle is much larger, the tracking accuracy requirement can be relaxed when the image is the dimmest.

Present indications are that 6 arc-second accuracies are possible on 9th magnitude stars using optics 3 inches in diameter. The weight of a two-telescope system with stable platform might be about 60 lb and its power requirement 40 watts.

Two tape recorders will probably be required, one to store the stellar monitor and star coordinate programs as commanded from CDA station, and one to store the angular and time data from the telescopes and clock. There has been no attempt to specify this equipment since the modest information rates involved make the requirement well within the state of the art.

A crystal clock will be standard equipment aboard Nimbus; a detailed description is given in Ref. 3. The clock has an accuracy of 10^{-7} or 20 bits, whereas 23-bit accuracy (one millisecond per orbit) is required if clock errors are to be unimportant. Calibration may possibly resolve the difficulty—if not, a better timing device must be employed. Since the output required for the refraction measurements is much less elaborate than for the Nimbus, an additional specialized clock for refraction purposes only might suffice.

The Nimbus telemetry system[3] could handle the refraction command and data acquisition requirements in a few seconds per pass. No additional telemeters would be required.

V. AN EMPIRICAL ATTEMPT TO TEST THE FUNDAMENTAL EQUATIONS

The Baker-Nunn camera on Mt. Haleakala, Maui, Hawaii is being utilized in measuring stellar refraction. This camera has 20" aperture and 20" focal length. The field of view is about 5° x 30° with a format 55 mm x 300 mm (approx.), which amounts to 406" per mm. The camera is a modified Schmidt and the film is stretched over a spherical sector with radius equal to focal length. Film can be transported rapidly and automatically from frame to frame and a time dial is photographed on each frame. Exposures may be taken every 2, 4, 8, 16, or 32 seconds automatically; the length of exposure equals one-fifth of this period.

Film is developed on Maui and sent to Cambridge for reduction with Mann comparators.

The camera can be pointed so that the optical axis is at + 1/2° altitude with the 5° field vertical. This means that the field extends from +3° down to -2°. The camera is located at an altitude of 3048 m, making the dip of the horizon 1°46'. Thus stars can be observed all the way to the horizon.

The method of obtaining refraction measurements is as follows.

Azimuth is set at 270° or nearly so, depending on the star field of most interest, and locked. Track angle (camera with respect to gimbal ring) is set at 90° and locked.

Altitude is set at 88-1/2° and an exposure is made. The film is advanced to the next frame and the camera altitude lowered quickly to 84-1/2°. Another exposure is taken 8.000 seconds after the first. The procedure is repeated and another exposure is made at altitude 80-1/2°, etc. Upon continuation of this procedure the 22nd frame will be exposed at 4-1/2° altitude.

Again the camera is lowered 4° to about + 1/2°. The transport mechanism is turned off and instead of a single exposure, 64 exposures are made on this frame. The shutter opens for 8/5 seconds every 8 seconds. A total exposure time of 64 x 8/5 = 102.4 seconds gives roughly an optimum background density. However, it is better to have the star images further apart than 8 seconds (time) of sidereal motion. Therefore, the operator holds a black flag in front of the aperture on every other shutter opening, making the exposures 16 seconds apart instead of 8. Also, prior to making the multiple-exposure frame the timing photography is set so that the time is recorded only on the first of the 64 exposures. These camera adjustments for the multi-exposed frame require time to perform; therefore the time interval between the 22nd and 23rd frames is 16.000 seconds.

By measurement of the 64 image positions of a star or stars and comparison with 64 calculated positions of an unrefracted image, the refraction as a function of ray height may be obtained.

In order to calculate an unrefracted star's position on the film, some connection between the celestial positions and the film coordinates must be made. If the film were very accurately positioned in the camera and the camera accurately positioned with respect to earth coordinates, this would be no problem. However, neither of these conditions hold: the film "frame" is not held fixed with respect to the camera mount within a few microns and the camera mount position circles can be read only to about ±6'. (In normal satellite tracking any star furnishes an origin for right ascension and declination coordinates and satellite positions are taken with respect to these. Refraction itself is of no consequence except for differential refraction between the star and satellite images. By choice of a star very near the satellite, differential refraction can be neglected.) This is the reason for the overlapping photographs from the zenith down to the final frame. Beginning at the zenith, the measured altitude difference between a star at the top of the frame and one at the bottom of the frame is compared with the actual altitude difference computed from a star catalog. The difference (subject to other corrections discussed later) is the refraction contribution between the two altitudes. The lower star of the first frame is on the top of the second frame; the refraction contribution between it and the star on the bottom of the second frame is found in the same manner. This process is repeated until the top of the final frame is reached. Summing all these individual refraction contributions gives the refraction of a star on the top of the final frame, with the following exception.

During the time between exposures sidereal motion has changed the altitudes of the stars, so that the refraction contribution of each of these small angles must also be added. All intervals except the last are 8 seconds; thus the sidereal motion is 120 arc seconds and the altitude change cannot be more. Since the altitude difference between the two measured stars on a frame averages 4°, the refraction contribution of this small angle amounts to less than 120"/4° = 1/120 of the principal contribution. Furthermore, this increment can be estimated very accurately, so the error due to these intervals is on the order of 1/1200. The final interval is 16 seconds and the error is doubled in this case. Unfortunately, the zenith angle is very great, so that this contribution to refraction completely overshadows the contributions near the zenith; therefore, we must allow the overall error to be considered doubled. The overall error in refraction angle due to non-zero intervals between frames is thus 1/600 or .17%.

A discussion of other corrections which may or may not be necessary will be deferred until the method of data reduction on the final frame has been discussed. Assume that the accurate refraction of a star image near the top of the frame is known. (It is assumed below that the star being used has its

first image near the top of the frame. It should be apparent that no difficulty arises in moving from star to star if necessary.)

The scheme is to measure the centers of the images of the film with a measuring engine which gives the coordinates in microns relative to an arbitrary reference on the film. Then a computation is made of each position on the film of the unrefracted star. The only reference between film and celestial coordinates is the image of the refracted star whose refraction is known.

Details of the computation are as follows.

A photographic film is obtained from the Baker-Munn station and for pictorial reasons has one star image on it, as shown in Fig. 13. The distance y_1'', measured from the horizontal axis of the film, locates the refracted star image and the distance y" positions the unrefracted image of the same star. The distance $y_1''-y''$ is then the deviation of a straight light ray from the refracted ray and by conversion to angular measure represents the refraction angle R as observed from the earth station.

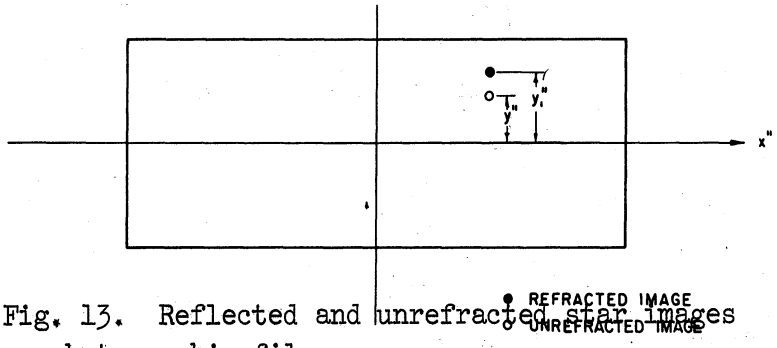

Fig. 13. Reflected and unrefracted star images on photographic film.

In order to calculate the distance y", these definitions are made:

d	declination
RA	right ascension of a star
L	latitude of the station
λ_s	longitude of the station measured east from Greenwich

λg GHA of the vernal equinox (function of time)

λ $= \lambda s + \lambda g$ - LHA of the vernal equinox

h altitude of the camera

Az aximuth of the camera

$\vec{S}$ unit vector pointing in the direction of a star

X inertial coordinate system

X' station coordinate system

X" film coordinate system

e_i, e'_i, e''_i $\quad i = 1,2,3$ $\quad\Big\{$ unit base vectors in the coordinate systems X, X', X"

x_i, x'_i, x''_i $\quad i = 1,2,3$ $\quad\Big\{$ components of the vector $\vec{S}$ in the coordinate systems X, X', X"

transformation equations from X to X' and X' to X" respectively

$$\begin{cases} x'_i = a_{ij}x_j & (48) \\ x''_k = b_{ki}x'_i & (49) \end{cases}$$

direction cosines between unit base vectors of the coordinate systems

$$\begin{cases} a_{ij} \\ b_{ki} \end{cases}$$

transformed coordinates of the vector $\vec{S}$ from X to X"

$$\begin{cases} x''_k = c_{kj}x_j & (50) \\ c_{kj} = b_{ki}a_{ij} & (51) \end{cases}$$

The components of $\vec{S}$ in the coordinate system X' are determined by relation (48) and the a_{ij}'s are obtained from the geometry of the orientation of the coordinate systems X and X', as shown in Fig. 14. The base vectors $\vec{e}'_3$ and $\vec{e}'_1$ satisfy the following relations:

$$\vec{e}'_3 = (\cos L \cos \lambda)\,\vec{e}_1 + (\cos L \sin \lambda)\vec{e}_2 + (\sin L)\vec{e}_3 \qquad (52)$$

$$\vec{e}'_1 = (-\sin \lambda)\vec{e}_1 + (\cos \lambda)\vec{e}_2 \qquad (53)$$

The vector $\vec{e}'_2$ is obtained by taking the cross product of $\vec{e}'_3$ and $\vec{e}'_1$ to form a right-handed triplet of base vectors:

$$\vec{e}'_2 = \vec{e}'_3 \times \vec{e}'_1 = \begin{vmatrix} \vec{e}_1 & \vec{e}_2 & \vec{e}_3 \\ \cos L \cos \lambda & \cos L \sin \lambda & \sin L \\ -\sin \lambda & \cos \lambda & 0 \end{vmatrix} \qquad (54)$$

$$\vec{e}'_2 = (-\sin L \cos \lambda)\vec{e}_1 + (-\sin L \sin \lambda)\vec{e}_2 + (\cos L)\vec{e}_3 \qquad (55)$$

The coefficients of these linear combinations are the a_{ij}'s. In matrix notation

$$a = \begin{pmatrix} a_{11} & a_{12} & a_{13} \\ a_{21} & a_{22} & a_{23} \\ a_{31} & a_{32} & a_{33} \end{pmatrix} \qquad (56)$$

$$\begin{aligned} a_{11} &= -\sin \lambda \\ a_{12} &= \cos \lambda \\ a_{13} &= 0 \end{aligned} \qquad (57)$$

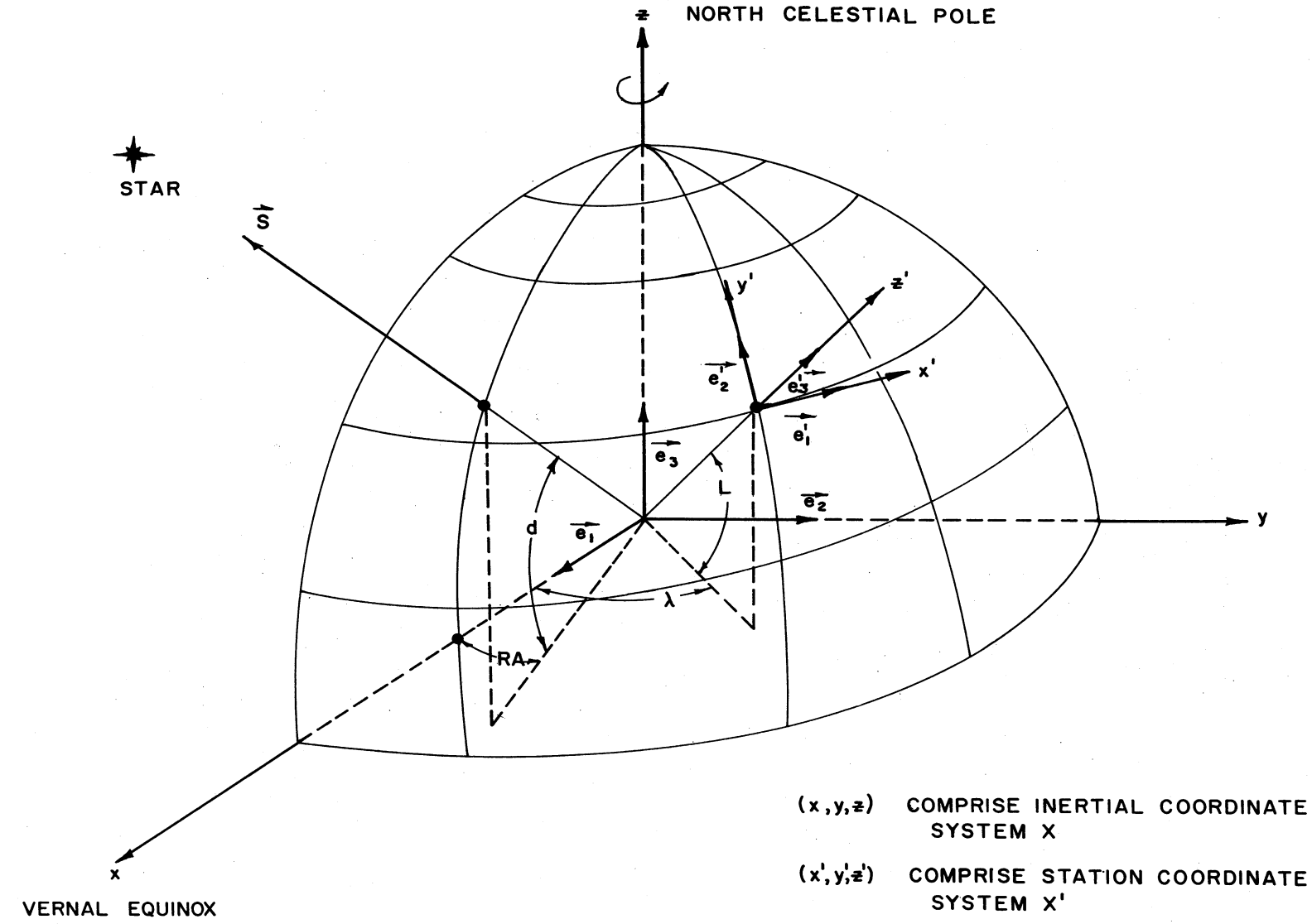

Fig. 14. Geometry of the orientation of coordinate systems X and X'.

$$
\begin{aligned}
a_{21} &= -\sin L \cos \lambda \\
a_{22} &= -\sin L \sin \lambda \qquad (58) \\
a_{23} &= \cos L
\end{aligned}
$$

$$
\begin{aligned}
a_{31} &= \cos L \cos \lambda \\
a_{32} &= \cos L \sin \lambda \qquad (59) \\
a_{33} &= \sin L
\end{aligned}
$$

By the same procedure, the b_{ki}'s can be determined for the transformation (49) between the coordinate systems X' and X", which are shown in Fig. 15.

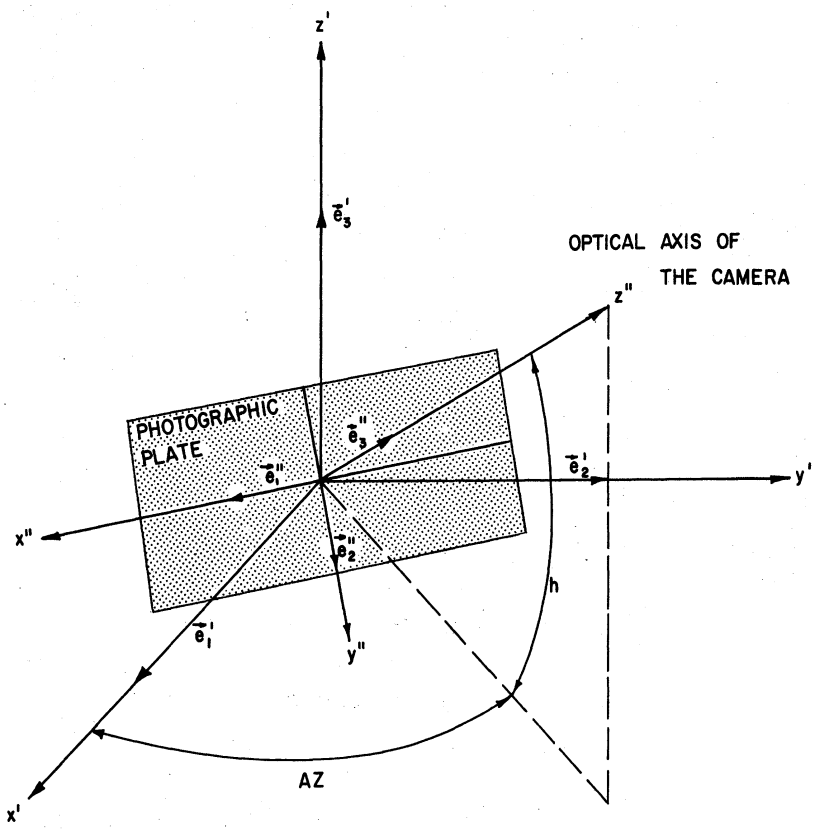

Fig. 15. Orientation of coordinate systems X' and X".

$$\vec{e}_3'' = (\cos Az \cos h)\vec{e}_1' + (\sin Az \cos h)\vec{e}_2' + (\sin h)\vec{e}_3' \tag{60}$$

$$\vec{e}_1'' = (\sin Az)\vec{e}_1' + (-\cos Az)\vec{e}_2' \tag{61}$$

$$\vec{e}_3'' \times \vec{e}_1'' = \vec{e}_2'' = (\cos Az \sin h)\vec{e}_1' + (\sin Az \sin h)\vec{e}_2' + (-\cos h)\vec{e}_3' \tag{62}$$

$$b = \begin{pmatrix} b_{11} & b_{12} & b_{13} \\ b_{21} & b_{22} & b_{23} \\ b_{31} & b_{32} & b_{33} \end{pmatrix} \tag{63}$$

$$\begin{aligned} b_{11} &= \sin Az \\ b_{12} &= -\cos Az \\ b_{13} &= 0 \end{aligned} \tag{64}$$

$$\begin{aligned} b_{21} &= \cos Az \sin h \\ b_{22} &= \sin Az \sin h \\ b_{23} &= -\cos h \end{aligned} \tag{65}$$

$$\begin{aligned} b_{31} &= \cos Az \cos h \\ b_{32} &= \sin Az \cos h \\ b_{33} &= \sin h \end{aligned} \tag{66}$$

The combined transformations (48) and (49) as expressed in Eq. (50) requires the matrix multiplication indicated in Eq. (51).

$$\begin{pmatrix} c_{11} & c_{12} & c_{13} \\ c_{21} & c_{22} & c_{23} \\ c_{31} & c_{32} & c_{33} \end{pmatrix} = \begin{pmatrix} b_{11} & b_{12} & b_{13} \\ b_{21} & b_{22} & b_{23} \\ b_{31} & b_{32} & b_{33} \end{pmatrix} \begin{pmatrix} a_{11} & a_{12} & a_{13} \\ a_{21} & a_{22} & a_{23} \\ a_{31} & a_{32} & a_{33} \end{pmatrix} \tag{67}$$

$$\begin{aligned} c_{11} &= -\sin Az \sin \lambda + \cos Az \sin L \cos \lambda \\ c_{12} &= \sin Az \cos \lambda + \cos Az \sin L \sin \lambda \\ c_{13} &= -\cos Az \cos L \end{aligned} \tag{68}$$

$$\begin{aligned} c_{21} &= -\cos Az \sin h \sin \lambda - \sin Az \sin h \sin L \cos \lambda - \cos h \cos L \cos \lambda \\ c_{22} &= \cos Az \sin h \cos \lambda - \sin Az \sin h \sin L \sin \lambda - \cos h \cos L \sin \lambda \\ c_{23} &= \sin Az \sin h \cosh L + \cos h \sin L \end{aligned} \tag{69}$$

$$\begin{aligned} c_{31} &= -\cos Az \cos h \sin \lambda - \sin Az \cos h \sin L \cos \lambda + \sin h \cos L \cos \lambda \\ c_{32} &= \cos Az \cos h \cos \lambda - \sin Az \cos h \sin L \sin \lambda + \sin L \cos L \sin \lambda \\ c_{33} &= \sin Az \cos h \cos L + \sin h \sin L \end{aligned} \tag{70}$$

An evaluation of these coefficients and the components of $\vec{S}$ which are expressed in terms of celestial coordinates

$$\begin{aligned} x &= \cos d \cos RA \\ y &= \cos d \sin RA \\ z &= \sin d \end{aligned} \tag{71}$$

will determine x", y", z" by these transformation equations (50)

$$
\begin{aligned}
x'' &= c_{11}x + c_{12}y + c_{13}z \\
y'' &= c_{21}x + c_{22}y + c_{23}z \\
z'' &= c_{31}x + c_{32}y + c_{33}z
\end{aligned}
\tag{72}
$$

The distance y" is, then, seen to be a function of the celestial coordinates of a star, the latitude and longitude of the observer, the orientation of the camera, and the time.

A multiple-exposure frame (Fig. 16) depicts a setting star. As the star sets, the light ray traverses atmospheric layers of increasing density and for equal exposure times the distance d between star images decreases due to increased bending of the ray denoted by the refraction angles R:

$$d_1 < d_2 < d_3 \ldots$$

$$R_1 > R_2 > R_3 \ldots$$

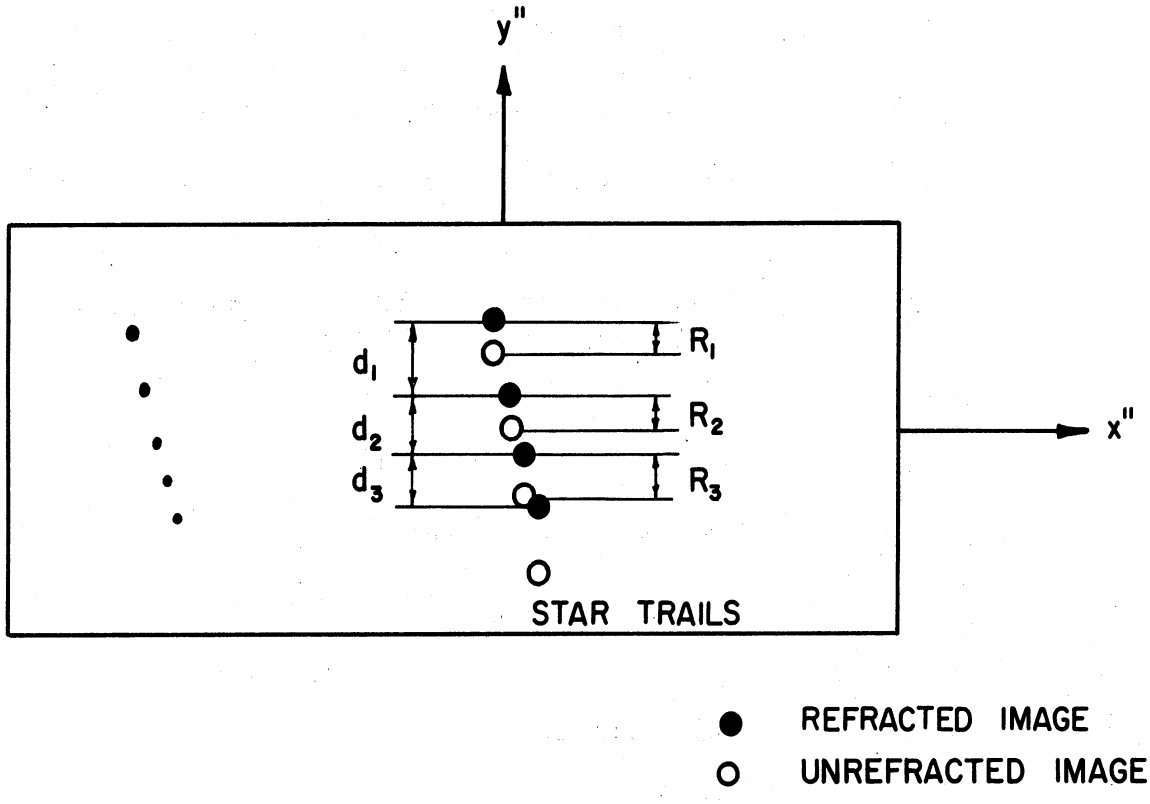

Fig. 16. Multiple-exposure frame depicting setting star.

However, the coordinates of the refracted star are not referenced to the x"y" axis of the film; therefore a subtraction, as indicated previously, is not sufficient to determine the refraction angles R. Thus if the refraction of the first image on the frame in Fig. 16 is known then together with the distance d between the refracted star images as measured and the position calculations of the unrefracted star y", all the succeeding refraction angles can be calculated.

The method of determining the refraction of the first image, which was described earlier, consists of taking overlapping photographs of the star field from an altitude angle of 90° down to the horizon (see Fig. 17). At 90°, a star may be considered an unrefracted reference star. The refraction angle of the star labeled 1 can now be calculated:

$$R_1 = d_1 - (y'' - y_1'') \tag{73}$$

Star 1 appears on the top of the 88-1/2° frame and since its refraction angle is known, the refraction of star 2 is given by

$$R_2 = d_2 - (y_1'' + R_1) - y_2'' \tag{74}$$

All succeeding angles are determined in this way from 90° down to the horizon frame. Summing these individual refraction contributions gives us the refraction of a star on the top of the horizon frame.

Presently, several refraction films are being reduced. No measurements are available at the time of writing.

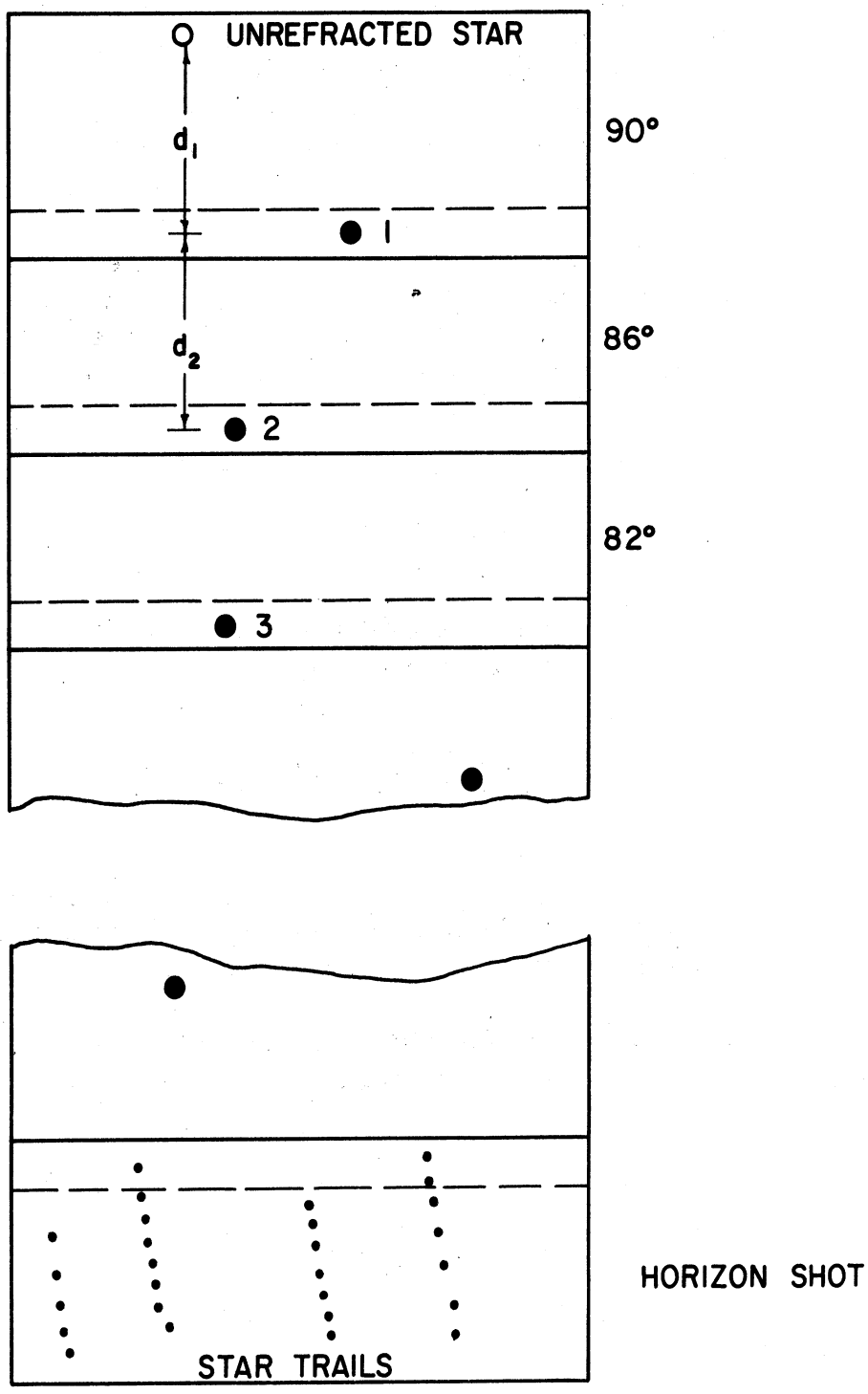

Fig. 17. Illustration of overlapping frames.

VI. ERRORS AND THEIR EFFECTS

The first results of the satellite refraction technique are the density profiles $\rho(h)$. These are not vertical profiles, but are nearly so at all except high azimuth angles (see Section II-D). The geographical positions (GP) of the highest and lowest ray tangencies are ordinarily close enough so that the difference is negligible. In any case the motion of the scan is readily calculable. For the purpose of this discussion, it is assumed $\rho(h)$ applies to a particular GP.

Errors in $\rho(h)$ arise from:

1a. angular errors in the tape recorded value of $R_s(t)$;

1b. time errors in the tape recorded value of $R_s(t)$;

2. errors in satellite position as a function of time;

3. errors in deducing $h_o(t)$; and

4. errors in retrieving the inverse function $\rho(h)$ from $R_s(h_o)$.

It is assumed that no errors arise from data storage or transmission and that errors in the location of the GP are negligible.

Errors 1a and 1b can be resolved into an error of refraction angle only. That is, if an absolutely correct refraction were measured at time t, but the time was presumed to be t_2, it can be assumed that the measurement was indeed made at t_2 and that the refraction angle is in error.

There are several sources for error in measuring the refraction angle: error in measuring real time on the satellite; error in recording the time simultaneously with the angular measurements; and error in the angular measurement due to the optical sensing equipment, from the optics through the digital encoder.

Preliminary investigation into equipment indicates that the state of the art in timing is such that the requirement for the nearest millisecond per orbital period can be met. It may thus be fair to assume the maximum timing error to be .0005 seconds. The time rate of change of refraction angle is greatest at the low end where dR/dt is approximately 2'/sec, so the maximum time error times the maximum angular rate gives only .06", a negligible error.

The angular error due to the sensing device itself, from optics through digital encoding, is strictly a function of the equipment which constitutes the heart of the system. The goal at present is ±6 arc seconds, which is considered quite realistic by several manufacturers of star-tracking equipment. The question of whether this goal will be attained or perhaps surpassed remains to be answered. Whatever the particular sources of error within the instrument, it may be that most are of an absolute magnitude independent of the size of the refraction angle. The expectation is, then, that the angular error should be negligible as a percent of refraction angle at the low end of the scan, that this angular error will become an increasingly important percentage of the refraction angle toward the beginning of the scan, and that it will eventually determine the upper limit of meaningful data.

The second error source considered is that involved in satellite tracking. Here again all errors can be resolved into one—an error in position at any given time. The position is required to draw the geometry of Fig. 2 as described in Section II-D. Reference to Fig. 2 will show that errors in satellite height times the sine of the altitude angle, and in the horizontal plane in the direction of the star times the cosine of the altitude angle, become errors in the distance $\overline{OB} = r_e+h_o+b$ and thus become errors in h_o. Since the altitude angle is roughly 30°, both sine and cosine are appreciable and errors in satellite position are translated virtually undiminished into errors of tangent height, h_o.

It appears that positional accuracy of 50 meters would be desirable. Since systems under development are reported to have even greater accuracy, this goal seems very reasonable. Tracking capability must also include rapid readout. Final, precise determination of position within one orbital period would be ideal. Longer delays mean simply that the data are passed to the meteorologists that much later. The improvement of tracking systems is beyond the scope of, although it is vital to, this project. It must be assumed that their development will be carried on by other agencies, and will ultimately be available for the refraction technique.

Errors in deducing the function $h_o(t)$ were discussed in Section II-D, where it was shown from Eq. (46) that one could reasonably assume any particular value of h_o to be correct ±90 meters. That analysis did not take into account the error in h_o due to satellite positioning error, since it assumed the geometry of Fig. 2 to be known. The satellite tracking error will be independent of the error in estimating μ_o, so there is a random combination of errors on the order of 50 and 90 meters in determining h_o. It is only fair to note that these are extreme conditions, the probable error being much less.

The last source of error cited, that of retrieving the function $\rho(h)$ from $R_s(h_o)$, is also mentioned in Section II-D, and some general conclusions are drawn from the form of Eq. (12).

In summary, a full scale error analysis has not been conducted because the final data reduction techniques have not been determined. Approximations have now been made to all necessary equations and the errors from each known source have been traced through the process independently. Errors due to the mathematical manipulation of the experimental data appear small. The most important errors will be those generated in the angular measuring device and in the determination of satellite position.

VII. CONCLUSIONS

The refraction technique has been studied with emphasis on areas where problems were anticipated. Solutions to these were obtained in several cases and indicated in others. No insurmountable problem was uncovered.

However, the area of equipment design has been scarcely examined, and the most crucial feasibility questions now lie in that domain.

In the immediate future, effort should be concentrated on:

1. Investigation into the feasibility of equipment design to meet the requirements of the refraction technique.

2. Numerical integration of the refraction function and development of an inversion technique for retrieving the density function.

3. Computer programming of the entire data reduction process to prove real time capability.

4. Completion of the ballistic camera refraction measurements and correlation with atmospheric conditions.

REFERENCES*

1. Jones, L. M., F. F. Fischbach, and J. W. Peterson, "Atmospheric Measurements from Satellite Observations of Stellar Refraction," University of Michigan ORA Report 04963-1-T, January 1962.

2. Jones, L. M., F. F. Fischbach, and J. W. Peterson, Satellite Measurements of Atmospheric Structure by Refraction," Planet. Space Sci., 9, 351-2, 1962.

3. Stampfl, R. A., The Nimbus Spacecraft and Its Communication System, NASA Goddard Space Flight Center Rpt. X-650-62-201, 1962.

See Also:

Bandeen, W. R., Earth oblateness and Relative Sun Motion Considerations in the Determination of an Ideal Orbit for the Nimbus Meteorological Satellite, NASA TN D-1045, July 1961.

Perkin-Elmer Corp., Long Focal Length Ballistic Camera Study. Eng. Rpt. 5942, October 1961.

*A comprehensive list of references on refraction and related topics is found in Reference 1.

APPENDIX A

COMPUTATION OF LATITUDE AND LONGITUDE OF RAY TANGENCY AND SUBSATELLITE POSITION AT OCCULTATION GIVEN A STAR AND AN ORBIT

For any unrefracted star the locus of points on the surface of the earth where the star appears on an observer s horizon, i.e., at altitude = 0°, or where the rays of light from the star are tangent to the earth s surface, there is a great circle, (SGC). The orientation of this great circle is unique with the star.

Now, for a satellite at a height h_s above the surface of the earth, the locus of points where the satellite might see the rays of light from the same star tangent to the earth's surface will be a circle of radius r_e, where r_e is the radius of the earth. The plane of this circle is parallel to and a distance W from the plane of the circle which is the locus of points where the light rays are tangent to the surface of the earth. The distance W between the planes is dependent directly on the height of the satellite—and for a satellite at height $h_s = 0$ the planes will coincide, i.e., W = 0. The geometry is shown in Fig. A-1.

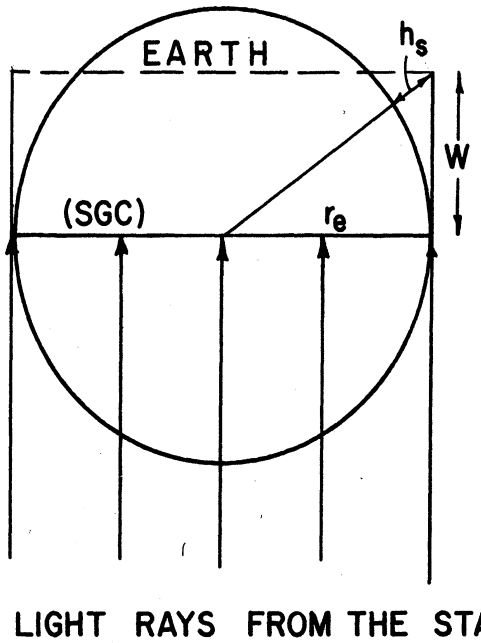

Fig. A-1. Geometry of unrefracted light rays.

The same general approach can be made for a star whose light is refracted by the atmosphere. The geometry, however, is slightly different, as indicated in Fig. A-2.

Two points on the satellite's orbit where it will "see" the rays of light

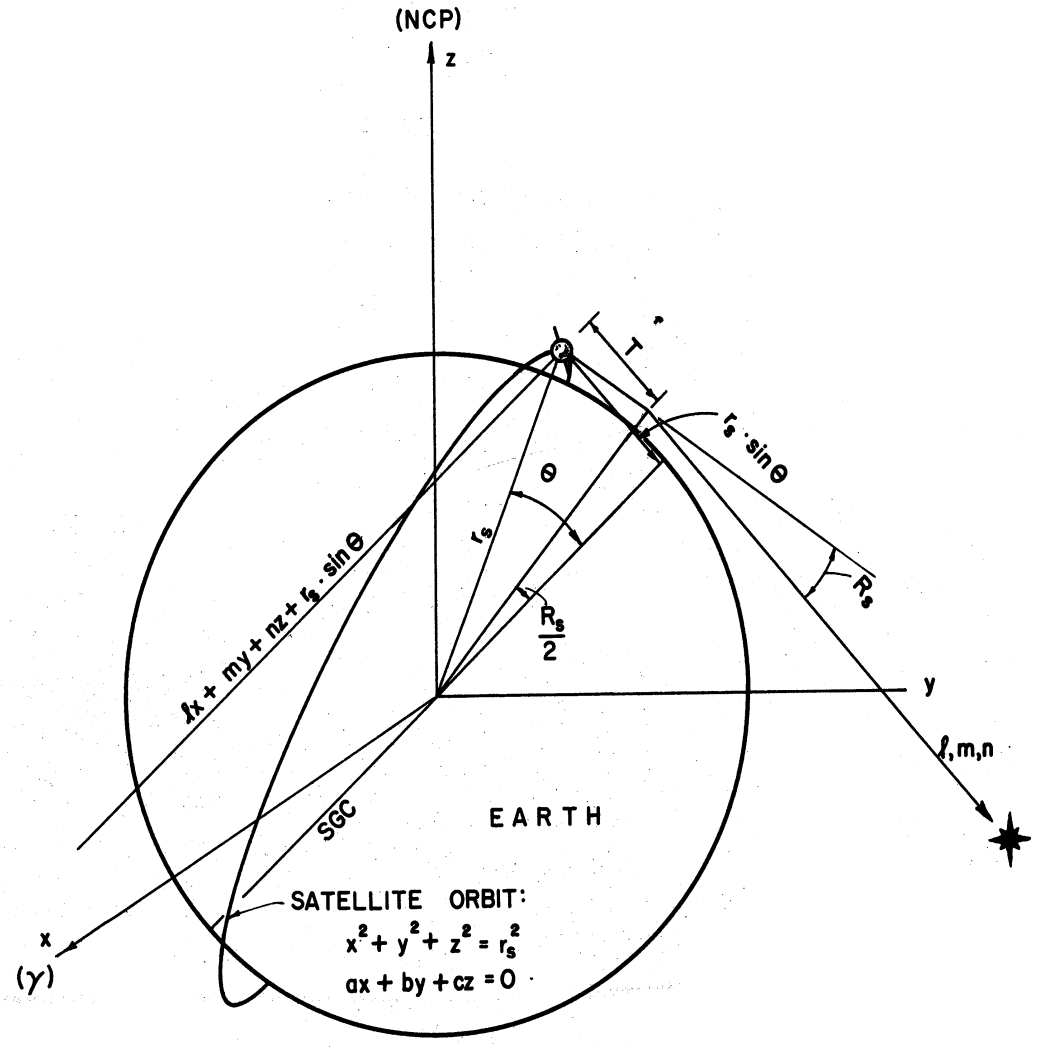

Fig. A-2. Geometry of occultation.

from the star tangent to the earth's surface can be obtained as the intersection points of the satellite's orbit and the circle that lies in the parallel plane a distance $r_s \cdot \sin\Theta$ from the plane which passes through the locus of points where the star's rays are tangent to the earth's surface.

The equation of the satellite's orbit is a solution of the equations

$$x^2 + y^2 + z^2 = r_s^2$$

$$ax + by + cz = 0$$

The coordinate system chosen is defined by the x axis positive in the direction of the vernal equinox, the z axis positive in the direction of the North Celestial Pole, and the y axis orthogonal to these axes. The letters a, b, and c are the direction numbers of the normal to the satellite's orbit.

The equation of the plane containing the circle which is the locus of points where the satellite will "see" the star's rays tangent to the surface of the earth is

$$lx + my + nz + r_s \cdot \sin \Theta = 0$$

where l, m, and n are the direction numbers of the normal to the plane containing the circle and are related to the right ascension and declination of the star under consideration as follows:

$$l = \cos \text{dec} \cdot \cos \text{RA}$$

$$m = \cos \text{dec} \cdot \sin \text{RA}$$

$$n = \sin \text{dec}$$

The simultaneous solutions of the equations

$$x^2 + y^2 + z^2 = r_s^2$$

$$ax + by + cz = 0$$

$$lx + my + nz + r_s \cdot \sin \Theta = 0$$

yields the following values of x, y, z, which define the two desired satellite positions:

$$x = \frac{-W[b\alpha + c\beta] \pm \sqrt{W^2[b\alpha + c\beta]^2 - [\alpha^2 + \beta^2 + \gamma^2][W^2(b^2 + c^2) - r_s^2 \gamma^2]}}{\alpha^2 + \beta^2 + \gamma^2}$$

$$y = \frac{-W[c\gamma - a\alpha] \pm \sqrt{W^2[c\gamma - a\alpha]^2 - [\alpha^2 + \beta^2 + \gamma^2][W^2(a^2 + c^2) - r_s^2 \beta^2]}}{\alpha^2 + \beta^2 + \gamma^2}$$

where

$$\alpha = bl - am$$

$$\beta = cl - an$$

$$\gamma = cm - bn$$

$$W = r_s \cdot \sin \Theta$$

z is calculated according to the following conditions:

If $c = 0$ and $n = 0$	then no calculation
If $c \neq 0$	then $z = (-ax - by)/c$
If $c = 0$, $a \neq 0$, $b \neq 0$, $x \neq 0$, $y \neq 0$	then $z = (-lx - my - W)/n$
If $c = 0$, $a = 0$, $b \neq 0$	then $z = (-lx - W)/n$
If $c = 0$, $a \neq 0$, $b = 0$	then $z = (-my - W)/n$

There are four possible combinations of x and y for which a value of z may be obtained. However, in order to obtain the setting point of the occulation, the following conditions must be satisfied:

$$lx + my + nz < 0$$

$$(bn - cm)x + (cl - an)y + (am - bl)z > 0$$

$$x^2 + y^2 + z^2 = r_s^2$$

In order to obtain the geographical position of the measurement use the values of x, y, z obtained in Eq. (1), then

$$x_{GP} = X + T \cdot l$$

$$y_{GP} = y + T \cdot m$$

$$z_{GP} = z + T \cdot n$$

where

$$T = r_s(\sin \Theta - \cos \Theta \cdot \tan R_s/2)$$

The satellite positions obtained in Eq. (1) are converted to latitude (β) and longitude (λ) by the equations

$$\beta = \arctan \frac{z}{x \cdot \sec(\lambda)}$$

$$\lambda = \arctan y/x$$

Longitude is measured eastward from the positive x-axis.

The latitude and longitude of the geographical position, β_{GP} and λ_{GP}, are obtained similarly:

$$\beta_{GP} = \arctan \frac{z}{x \cdot \sec(\lambda_{GP})}$$

$$\lambda_{GP} = \text{arc tan } y/x$$

The coordinate system based on the satellite is oriented such that the x' axis is positive in the direction of the orbital motion of the satellite, the z' axis points in the direction of the satellite's zenith, and the y' axis is orthogonal to these axes. The transformation from unprimed to primed coordinates is accomplished with the following equations:

$$x' = \cos \text{dec} \cos \text{RA}(b \cos \beta - c \cos \beta \sin \lambda) + \cos \text{dec} \sin \text{RA}(c \cos \beta \cos \lambda - a \sin \beta) + \sin \text{dec}(a \cos \beta \sin \lambda - b \cos \beta \cos \lambda)$$

$$y' = a \cos \text{dec} \cos \text{RA} + b \cos \text{dec} \sin \text{RA} + c \sin \text{dec}$$

$$z' = \cos \text{dec} \cos \text{RA} \cos \beta \cos \lambda + \cos \text{dec} \sin \text{RA} \cos \beta \sin \lambda + \sin \text{dec} \sin \beta$$

The relations

$$\theta = \text{arc tan} \frac{z'}{x' \sec \phi + R_S}$$

$$\phi = \text{arc tan } y'/x'$$

then give the altitude, θ, and the azimuth, ϕ, of the star in the primed or satellite-based coordinates.

APPENDIX B

ATMOSPHERIC ATTENUATION OF STARLIGHT

by Maurice E. Graves

I. INTRODUCTION

When a ray of starlight penetrates the earth's atmosphere, it suffers a significant diminution of intensity. This diminution is caused by refraction within the density stratification of the medium, plus the effective presence of certain constituents which scatter or absorb the radiant energy. These constituents include water in all three phases, ozone, dust and haze particles and the gas molecules of the atmosphere. In this report, we will discuss the relative importance of these attenuating agents with regard to horizontal, grazing beams passing through the atmosphere at minimum heights under 30 km.

Some of the major contributions to these fields have come from Europeans, viz., Link,[8] who has written upon attenuation by refraction, and Schoenberg,[14] Van de Hulst[17,18] and Waldram,[19] who have written extensively on light scattering and absorption within the atmosphere. Other material on the latter two topics are to be found in Johnson,[4] Lillestrand et al.[7] and Middleton.[11]

The dearth of measurements of attenuation for horizontal rays at the earth's surface and aloft necessitates the use of theoretical results. However, the formulae should indicate which attenuators are important, and they give useful estimates of the amount of dimming caused by a particular agent. Tables 139-158 in List[9] and the Light-scattering Coefficients in Boll, Leacock, Clark and Churchill[2] will be employed to give quantitative results.

II. ATTENUATION BY REFRACTION

Jones, Fischbach and Peterson[5] have pointed out that the refraction of horizontal starbeams reduces the intensity of starlight at an observation point outside the atmosphere, e.g., at a satellite, by a factor which exceeds 10 for a ray tangent to the earth's surface. Thus, the apparent magnitude of Sirius, when very near the horizon, is diminished by $10.6 \times 100^{-1/5}$ magnitudes, or from -1.6 to +2.2.

The reduction factor is: $S = 1 + R_s x/H$, where

R_s = refraction angle in radians for a complete horizontal traverse

x = path length from satellite to minimum height of ray

H = scale height

This formula for S can be traced to Link,[8] who used it to study the atmospheres of planets when they occult bright stars. It is important to note that x is the distance from the data point to the satellite, and that it can be taken as constant for a particular satellite altitude (see Fig. B-1). Taking x = 3900 km for a satellite altitude of 1100 km, and taking H = 7.5 km, we find the following variation of transmission ratio I/I_o vs. height of ray perigee h_o (see Fig. B-2), where

I = intensity of star ray after penetration

I_o = intensity of star ray prior to entry

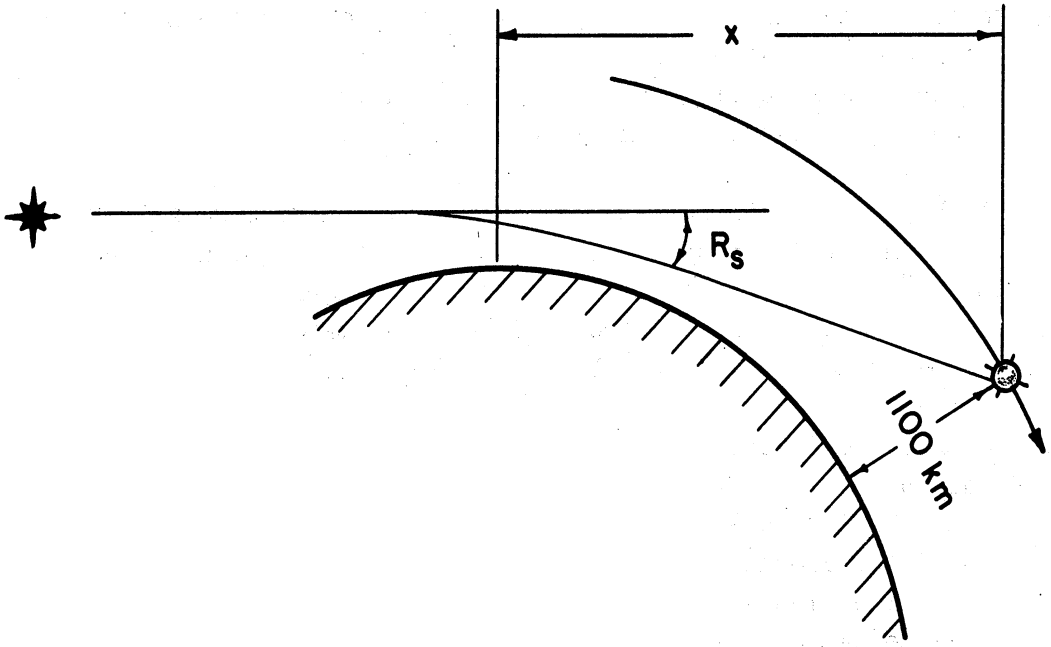

Fig. B-1. Geometry of attenuation by refraction.

III. SCATTERING

Confining our study to the optical range of wave lengths, 0.4μ to 0.7μ, we will follow Van de Hulst's definitions of basic terms, which give:

Attenuation = extinction = scattering + absorption

In considering the effects of scattering, some simplifying assumptions are necessary, namely:

1. Scattered light retains the same wave length as incident light.

2. In the case of Mie scattering by small particles, the particles are independent, e.g., their mutual distance apart is at least 3 times their radii.

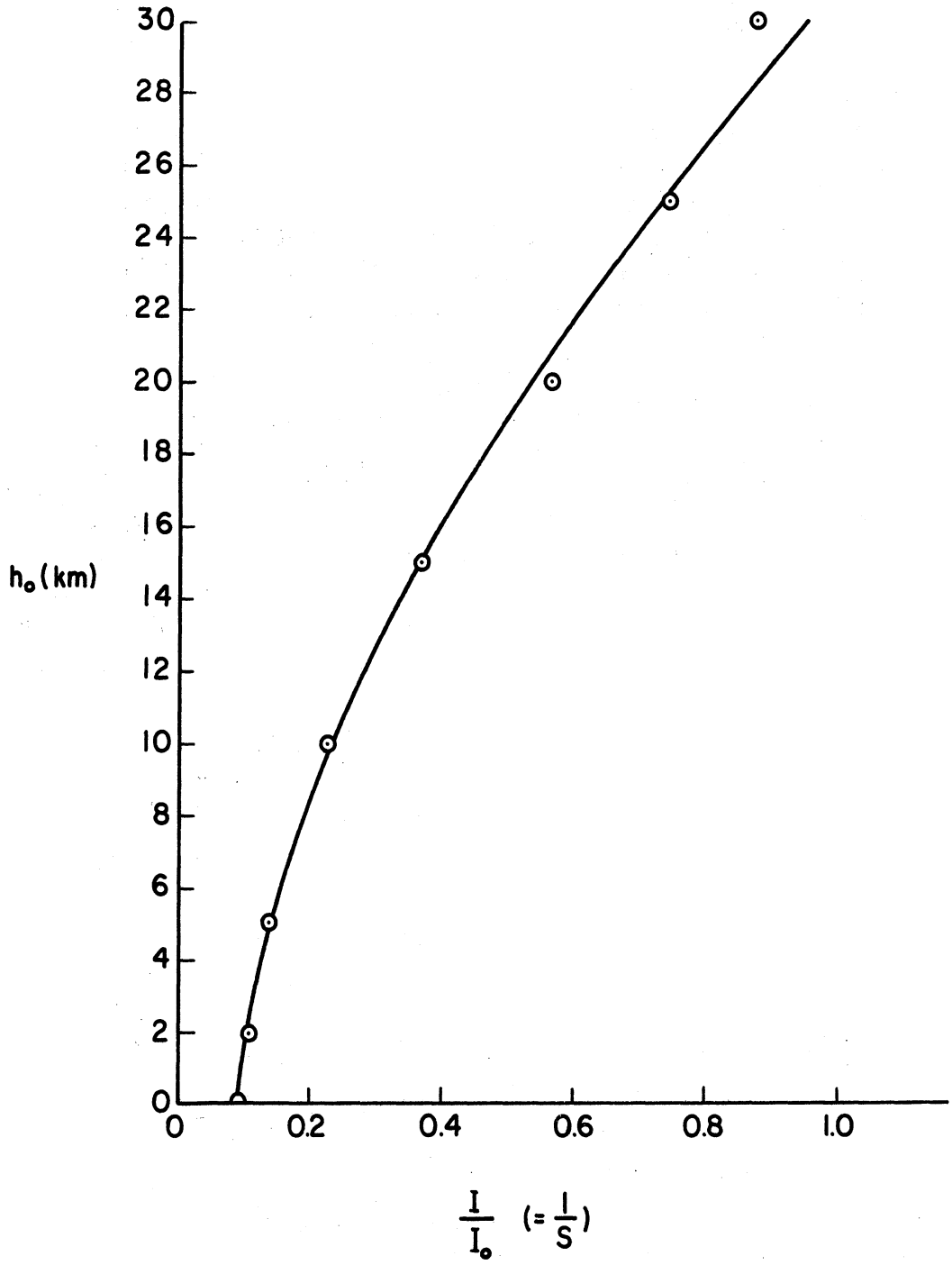

Fig. B-2. Transmission ratio I/I_0 as a function of ray perigee h_0.

3. All scattering is single rather than multiple. Thus, the radiation reaching a particular particle or molecule is essentially that of the original beam.

Taking up Rayleigh (molecular) scattering first, we find that the ratio of I/I_o introduced above can be equated to an expression, $e^{-b \sec z}$. Schoenberg[14] states that $b = 32\pi^3(\mu - 1)^2/3N\lambda^4$, where μ = refractive index of the air = f(h) and N = number of molecules/cm^3. When z is greater than 80°, however, $e^{-b \sec z}$ becomes inapplicable because of the behavior of the secant function, and the ray's curvature (2.96×10^{-5} km^{-1}) and earth's curvature (1.57×10^{-4} km^{-1}) must be considered when nearing z = 90°. Furthermore, μ is not easy to evaluate as f(h).

These difficulties have been met by Lillestrand et al.[7] in the following way:

1. Compute the optical air mass, which is the mass of air, m(h,z), in a volume of unit cross section, starting at height h, taken in a direction z degrees from the zenith.[13] The formula applicable for $z < 80°$ is simply $m(h_o,z) = m(h_o,0°) \sec z$; for greater z values Pressly[13] uses

$$m(h,z) = \int_{h_o}^{220 \text{ km}} \frac{\rho(y)}{\left[1 - \left(\frac{R_o + z}{R_o + y}\right)^2 \sin^2 z\right]^{1/2}} \, dy$$

where $\rho(y)$ = density along the path and R = radius of the earth = 6368 km.

2. Rewrite the Rayleigh expression for I/I_o, $e^{-b \sec z}$, as

$$I/I_o = 10^{-kmp/p_o}$$

where k = f(λ), m = number of unit vertical air masses, and the pressure p, like m, is f(h). Then, following Moon,[12] one can utilize experimental results such as Fowle's[3] for $(I/I_o)_{z=0}$ in a vertical column above a mountain summit. Thus, setting m = 1 for z = 0 and setting $p = p_o$ to solve for k in the equation $I/I_o = 10^{-k}$, Moon plots k vs. λ and then obtains a numerical value for k_1 (=0.00380) such that $(I/I_o) = k_1\lambda^{-4}$. The exponent of "-4" on λ corresponds to a slope of -4 when k is the ordinate, and this agrees with Rayleigh's original expression for b, where $b \propto -4$.

3. Plot I/I_o against h, using λ as a parameter.

Following a procedure used by Lillestrand et al.,[7] we have done this for

$z = 90°$ for molecular scattering, and have obtained the transmissivities shown in Table B-I.

TABLE B-I

I/I_o IN PERCENTAGE TRANSMISSION (MOLECULAR SCATTERING)

h_o(km)	$\lambda = 0.4\mu$	0.5μ	0.6μ	0.7μ	$\sum I/I_o$*
0	0	0	1	8	1
5	0	5	24	46	16
10	16	47	70	82	56
15	68	85	93	96	86
20	92	97	98	99	96
25	100	100	100	100	100

*Integrated effect found by counting squares.

The notable dependence of I/I_o on λ in Table B-I may also be seen by making a simple calculation for red and violet light components, thus:

$$\text{red light: } \lambda = 0.7\mu$$
$$\text{violet light: } \lambda = 0.4\mu$$

$I/I_o \propto \lambda^{-4}$; therefore the atmosphere removes $(0.7/0.4)^4 \approx 10$ times as much violet light as red light through molecular scattering.

Although water vapor consists of gas molecules, Moon[12] finds that true Rayleigh scattering is not operative in this case. Fowle[3] had separated the water vapor effect in his Mount Wilson data, and in plotting k vs. λ graphically, Moon obtains a $k_1 = 0.0075$ and $(I/I_o)_{z=0} \propto \lambda^{-2}$, rather than λ^{-4}.

To make a table for water vapor scattering similar to Table B-I, we have assumed $(I/I_o) = 10^{-km\, w/w_o}$ where

w = amount of precipitable water in mm

w_o = amount of precipitable water in mm at the surface

m = number of air masses; $m = 1$ for $h = 0$

$k = k_1 \lambda^{-2}$

Assuming a value of $w_o = 20$ mm along with Moon, and a decrease of w from w_o at $h = 0$ to 5 mm at $h = 5$ km to 0 mm at $h = 10$ km, we have obtained Figure B-3 and Table B-II for water vapor.

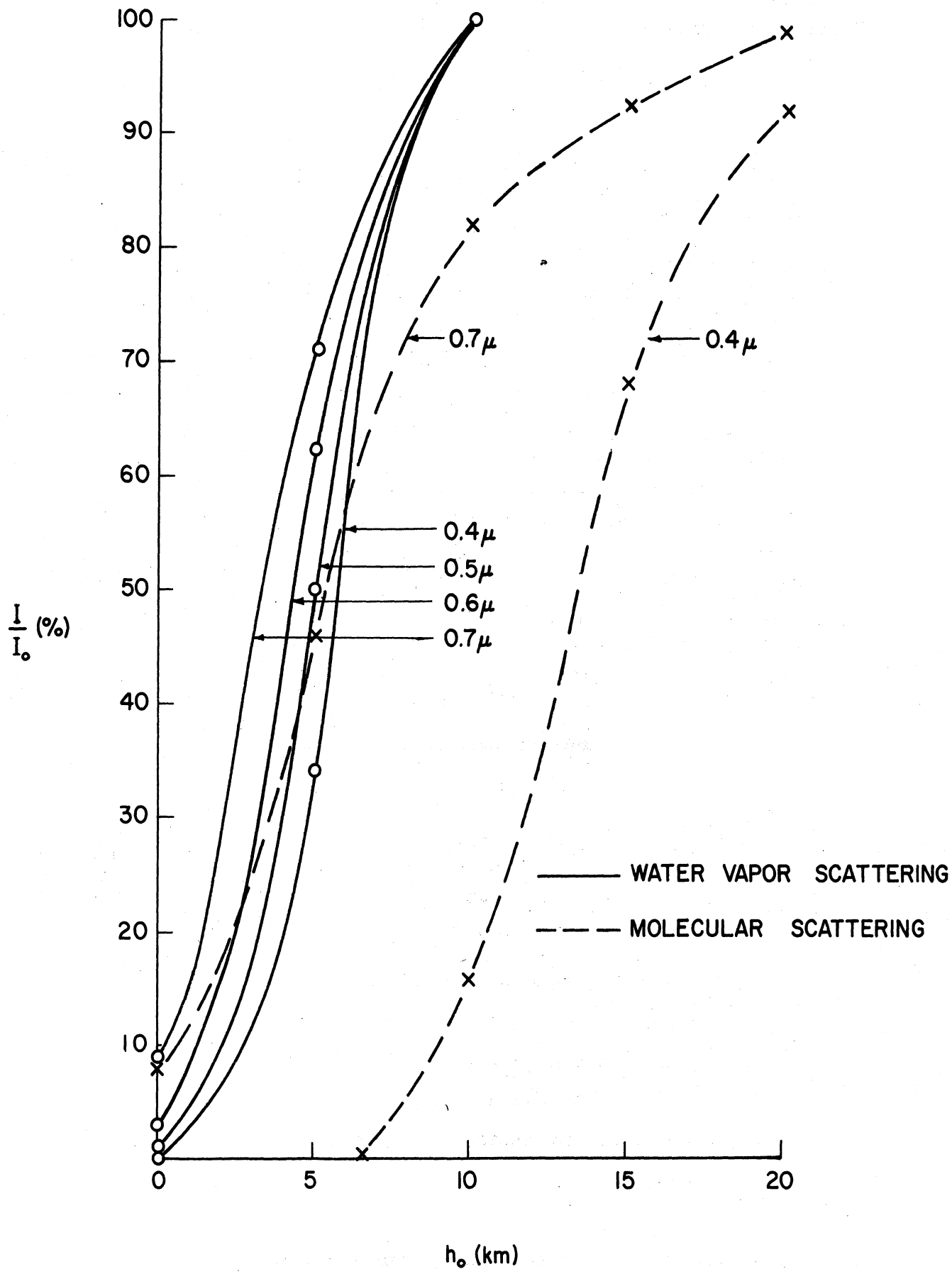

Fig. B-3. Percentage transmission I/I_0 at various optical wavelengths as a function of ray perigee h_0, for water vapor and molecular scattering.

TABLE B-II

I/I_o IN PERCENTAGE TRANSMISSION (WATER VAPOR SCATTERING)

h_o(km)	λ = 0.4μ	0.5μ	0.6μ	0.7μ	$\sum I/I_o$*
0	0	1	3	9	6
5	34	50	62	71	51
10	100	100	100	100	100
15	100	100	100	100	100
20	100	100	100	100	100

*Integrated effect found by counting squares.

Sample computations are as follows:

$$\lambda = 0.4\mu$$
$$h_o = 5 \text{ km}$$
$$w/w_o = 5/20 = 0.25$$
$$m = 2(2.14 \times 10^8/1.07 \times 10^7) = 40$$
$$k = 0.0075/(0.4)^2 = 0.047$$
$$I/I_o = 10^{-kmw/w_o}$$
$$= 10^{-0.470}$$
$$= 0.339$$

$$\lambda = 0.7\mu$$
$$h_o = 10 \text{ km}$$
$$w/w_o = 10/20 = 0.50$$
$$m = 2(1.10 \times 10^8/1.07 \times 10^7) = 20.6$$
$$k = 0.0075/(0.7)^2 = 0.015$$
$$I/I_o = 10^{-0.154}$$
$$= .702$$

A 20 mm depth of precipitable water is typical of a maritime tropical air mass, and the sample calculations given above show a significant low-level scattering effect due to water vapor. The λ = 0.4μ and λ = 0.7μ curves for molecular scattering in a Standard NACA Atmosphere have been recomputed and entered in Fig.

B-3 for comparison with water vapor scattering.

In addition to molecular and water vapor scattering, there remains the possibility of scattering by liquid water and by solid particles such as dust, haze or ice crystals. An attempt to evaluate the effects of dust and haze was made by Moon,[12] who compared the combined curve for molecular scattering and 20 mm precipitable water with a mean curve for overall scattering obtained at Washington, D. C. by the Smithsonian Institution.[15] Assuming that dust and haze particles account for the difference between the curves, a third scattering coefficient was obtained, with $k_1 = 0.0358$.

To find some approximate values for dust and haze, one needs to assume a probable distribution of particle count with height. There is indirect evidence of nuclei in the stratosphere, as well as lower levels, seen in the occurrence of noctilucent and mother-of-pearl clouds, attenuation associated with meteor showers, twilight phenomena and high level "dust horizons." Direct measurements have also been completed by the use of rockets, as by Junge, Chagnon and Manson[6] in the Northern Plains States. The Aitken nuclei counter and impactor used by these investigators gave the average particle concentrations between 7 and 25 km in the stratosphere and upper troposphere. A separation of the particles into size ranges gives the results shown in Table B-III.

TABLE B-III

AVERAGE PARTICLE CONCENTRATIONS IN STRATOSPHERE AND TROPOSPHERE

Radius of particle (μ)	< 0.1	0.1-1.0	> 1.0
Average concentration (cm^{-3})			
Stratosphere, 25 km	6	0.1	0.01
Troposphere, 7 km	variable	1-5	1-5

Since the mean overall scattering curve to be compared is for Washington, D. C., a mean surface particle concentration must be assumed for the same locality. In 1937, such a mean value was estimated at 800 cm^{-3}, so we can proceed as before with $(I/I_o)d = 10^{-kmd/d_o}$ where

d = concentration of particles per cm^3

d_o = concentration of particles per cm^3 at surface.

In this case, the graphical analysis by Moon[12] yields a $k_1 = 0.0358$ and $(I/I_o)_{z=0} \propto \lambda^{-0.75}$; thus there is still some dependence upon wave length despite the larger size of the scattering agent. Table B-IV gives the transmission factors computed for haze particles with radii < 0.1 μ and the concentration of

particles decreasing from 800 cm^{-3} at the surface to 100 cm^{-3} at 5 km to 10 cm^{-3} at 10 km.

TABLE B-IV

I/I_o IN PERCENTAGE TRANSMISSION (HAZE PARTICLES WITH RADII < 0.1 μ)

h_o(km)	λ = 0.4μ	0.5μ	0.6μ	0.7μ	$\sum I/I_o$*
0	6	3	2	1	3
5	81	78	76	73	77
10	99	99	99	98	99
15	100	100	100	100	100

*Integrated effect found by counting squares.

Particles with radii exceeding 0.1μ are too infrequent to contribute an appreciable amount to Table B-IV.

The "Bouguer Relation" noted by Middleton[11] may be used to accumulate the scattering effects of molecules, water vapor and dust. This formula is based upon experimental evidence, and it merely combines terms to give

$$I/I_o = [10^{-0.00380\,\lambda^{-4}\,p/p_o - 0.0075\lambda^2\,w/w_o - 0.0358\lambda^{0.75}\,d/d_o}]^m$$

When we perform this computation for specific λ and h_o values as before, we obtain Table B-V

TABLE B-V

I/I_o IN PERCENTAGE TRANSMISSION (TOTAL SCATTERING EFFECT OF AIR MOLECULES, WATER VAPOR AND DUST)

h_o(km)	λ = 0.4μ	0.5μ	0.6μ	0.7μ	$\sum I/I_o$*
0	0	0	0	0	0
5	0	2	11	23	9
10	16	46	69	81	53
15	68	85	93	96	85
20	92	97	98	99	97

*Integrated effect found by counting squares.

From 5 km upward, there is a pronounced improvement of transmissivity with increase in wave length in the visible range.

The above computations are based upon the formulae and assumptions for Rayleigh scattering. Dust particles of the order of 1μ in diameter are larger than optical wave lengths and one should seek to apply Mie theory to arrive at some representative values for I/I_o. Boll, Leacock, Clark and Churchill[2] have published tables for a scattering coefficient, K, in the relation, $I/I_o = e^{-KnLd^2/4}$ where

n = number of particles per cm^3

L = path length in cm*

d = diameter of particles, which are assumed to be spherical and uniform in size

$K = f(\alpha, m)$, where $\alpha = \pi d/\lambda$ and m = index of refraction of the particles relative to the surrounding media.

The results depend a great deal on the choice of m. For the stratosphere near an altitude of 18 km, these tables yield the following values for the observed concentration reported by Junge, Changnon and Manson:[6]

d = 1.0μ

λ = 0.4μ

$\alpha = \pi d/\lambda = 7.8$

$L = 2.5 \times 10^8$ cm

$n = 0.1\ cm^{-3}$

m = 0.60
K = 1.89, from table[2] } I/I_o = 69.1%

m = 0.90
K = 0.90, from table[2] } I/I_o = 83.5%

These transmissivities are notably lower than the high values obtained for the stratosphere in Table B-IV. The K values do not diminish indefinitely with increase in m, excepting when $\alpha < 1$.

With regard to water droplets with diameters up to 10μ, Mie scattering area coefficients are given in List.[9] In this case, the formula suggested for

*h_o(km)	0	5	10	20	30
L($\times 10^8$ cm)	3.0	3.0	2.8	2.4	2.0

I/I_o is

$$I/I_o = e^{-\sum \pi n k_s L d^2/4}$$

where the summation is taken over all sizes of spheres present. The result for a typical fair weather cumulus cloud top with L = 100 ft (3×10^4 cm) is, according to raindrop size spectra listed in Mason,[10]

$$I/I_o = e^{-(225\ cm^{-3})(14 \times 10^{-4} cm)^2(2.0)(3 \times 10^3\ cm)/4}$$

$$\cdot\ e^{-(60\ cm^{-3})(24 \times 10^{-4}\ cm)^2(2.0)(3 \times 10^3\ cm)/4} \cdots$$

$$= e^{-2.08\ -\ 1.62\ -\ \cdots}$$

$$< 0.025$$

The concentrations of cloud droplets commonly exceed 300 cm^{-3} in stratiform clouds, so droplet scattering appears to be 100% effective for most cloud types, even when the path length through the cloud is of the order of 10^2ft.

Ice crystals of decidedly nonspherical form displace liquid droplets as the hydrometeoric scattering agent at altitudes of 15 km or less, depending upon the season and the latitude. The irregularity of such crystals creates an extremely complex problem which cannot be solved by convenient groupings of particle sizes as before. However, it does seem probable that the I/I_o ratios with which light is transmitted through ice crystal clouds are not appreciably greater than the I/I_o ratios with which it is transmitted through the water droplet types discussed above.

IV. ABSORPTION

Attenuation was defined in Section III as the combined effects of scattering and absorption. Some of the possible absorbing agents are water vapor, CO_2, ozone, oxygen, liquid water, ice crystals, dust and haze.

The absorption bands of water vapor, CO_2 and oxygen do not lie in the optical wave lengths and absorption of light by liquid water and ice crystals is negligible in clouds in comparison to the scattering effect. This leaves only ozone to be evaluated. In the visible range, we find the coefficient, k, in the familiar expression $I/I_o = e^{-k\Delta z}$, increasing from about zero at 0.4μ to 0.05 at 0.6μ and then decreasing.[9] This coefficient applies to a layer of pure ozone Δz cm thick at the surface, and its smallness indicates that we can probably omit ozone from the list without introducing much error.

It appears, then, that there are no absorbing agents of any consequence in the visible range with the possible exceptions of dust and haze. No evidence on the absorbing qualities of these aerosols has been located as yet.

V. DISTRIBUTION OF EFFECTIVE SCATTERING AGENTS

The effective light scatterers were found to include the basic, gaseous atmosphere, water vapor, dust and haze, liquid water droplets and ice crystals. The distribution of the last three items is not very well known. However, some comments will be made on each of the five scattering agents.

A. Basic Gaseous Atmosphere

The composition of the atmosphere is sufficiently uniform to permit the results in Table B-I to be generally applicable. Since we are dealing with horizontal rays, spherical stratification is also assumed tacitly when Table B-I is used.

B. Water Vapor

Statements about the distribution of water vapor, e.g., precipitable water, must be largely qualitative. The serious attenuation of starlight in the humid tropics has long been noted by the writer, and it is largely in this region that the larger values of 20-30 mm will be found frequently. However, outside of the Intertropical Convergence Zone* and the deep moist layers of tropical disturbances, the high moisture values will often cut off at 3-4 km, making the figures for 5 and 10 km in Table B-II somewhat low. On the other hand, in the deep moist layers which invade the middle latitudes, the actual effect of water vapor will probably exceed these figures. In high latitudes, the precipitable water will be much less, making Table B-II unrepresentative there.

C. Dust and Haze

The surface concentration of solid particles may exceed 50,000 cm^{-3} at times, denoting great variability in lower levels, and one cannot assume a linear decrease with height because of the tendency for particles to congregate at the bases of temperature inversions. Thus the tropopause is a susceptible haze level, the range of tropopause altitude being as in Table B-VI.

*The Intertropical Convergence Zone (ITC) extends almost continuously around the earth within ± 15° of the Equator.

TABLE B-VI

RANGE OF MEAN TROPOPAUSE ALTITUDE

Latitude	Altitude of Mean Tropopause
0 - 25°	16 km
25 - 60	10 - 16
60 - 90	8

As a first approximation, we may take the data of Junge, Changnon and Manson[5] from the Northern Plains States to be representative of the dust and haze distribution in the mean over the continents. The surface value used may be too great for the air over the oceans.

D. Liquid Water Droplets and Ice Crystals

The high attenuation rate found above for clouds signifies that poor penetration can be expected from cloud-obstructed light. Therefore the presence of small cumulus towers can evidently interrupt a starbeam as surely as a stratified layer, and the great frequency of clouds in the lower and middle troposphere causes much light extinction. The distribution of the higher, cirriform clouds is of interest here, but it is only partly known because ground observers miss seeing over 50% of the true occurrence and aircraft observations are scarce.

Stone[16] has analyzed the following data to arrive at some of the characteristics of cirriform cloud distribution:

(a) Double-theodolite measurements taken during the International Cloud Year, 1896-1897

(b) 176 British aircraft observations, 1949-1954

(c) 2000 Canadian aircraft observations, 1950-1955

(d) 700 USAF aircraft observations, 1954-1955.

Appleman[1] has analyzed 1375 Western European aircraft observations, 1950-1957, along with the above observations. The two studies yield the following conclusions regarding upper cloud distribution:

1. Nontropical Regions

(a) The percentage occurrence of cirriform clouds ranges from 15 to 30%.

(b) The modal height of the bases in high latitudes is 7 km. The modal height in low latitudes is 12 km. There is a linear variation between high and low latitudes.

(c) The seasonal range of modal height over Canada is < 2 km.

(d) The thickness is < 2 km in a majority of cases, but thickness has occasionally exceeded 5 km. The mean thickness is 6000 ft.

(e) Cirrus usually becomes layered when thickness exceeds 3 km.

(f) Most cirrus tops are 3000 to 5000 ft below the tropopause.

2. Tropical Regions

(a) There is an abundance of cirriform clouds flowing out from the Intertropical Convergence Zone. Their bases are frequently reported by airline pilots to be above 12 km. In and near the ITC, these clouds must have a percentage occurrence of 50% or more at 12-16 km. Their origin is due to ascending moist air, particularly in heavy cumuli which have a nocturnal maximum over the oceans.

(b) Stratospheric occurrence of cirrus has been reported occasionally in middle latitudes, but hardly at all in high or low latitudes. Such frequency is possible where there is sufficient moisture and vertical motion, but favorable conditions are seldom found above the tropopause.

VI. CONCLUSIONS

The attenuation of a ray of starlight within the earth's atmosphere is caused by (1) refraction into a solid angle, and (2) scattering by air molecules, water in any form and haze or dust particles. Absorption by the above scattering agents and other gases is found to be negligible, with the possible exception of haze and dust.

Some representative, quantitative results for these attenuators are summarized in Table B-VII for the integrated waveband from 0.4μ to 0.7μ. In this table it is more convenient to present the quantity $1 - I/I_o$, the percentage reduction of the beam intensity, rather than I/I_o. A ray path through the entire atmosphere parallel to a tangent grazing ray is considered for heights of 0, 5, 10, 15 and 20 km.

TABLE B-VII

PERCENTAGE REDUCTION OF A HORIZONTAL RAY DUE TO ATTENUATING AGENT

	h_o (kilometers)					
	0	5	10	15	20	25
Refraction (constant	91	86	78	63	46	27
Scattering						
Molecular (constant)	99	84	44	14	4	0
Water vapor (variable)	94	49	0	0	0	0
Haze and dust (variable)	97	23	1	0	0	0
Bouguer Relation	100	91	47	15	3	0
Water droplets (100 ft or more of cloud)	100	100	100	100	100	100
Ice crystals (ditto)	100	100	100	100	100	100
Absorption	0	0	0	0	0	0

The values computed by the Bouguer Relation summarize, in effect, the first three items under "Scattering," and can be changed to the form of stellar magnitude reduction. Fig. B-4 gives the curve used for this purpose, whereby a reduction factor of $100^{1/5}$ (=2.512) in light intensity equals a decrease of 1.0 in apparent magnitude.

Table B-VIII gives the converted values from Table B-VII for individual scattering agents and for the Bouguer Relation for combined scattering effects. The latter formula's 100% attenuation at $h_o = 0$ presents a problem, but if the magnitude reduction curves are drawn for each component of the Bouguer Relation, as in the inset of Fig. B-IV an extrapolation to $h_o = 0$ analogous to the three lower curves gives a magnitude diminution of about 10 at the surface. Thus the total effect of attenuation at a satellite's vantage point ranges from 10 magnitudes for a surface grazing ray, to 0.2 magnitude for a ray with a minimum tangent height of 25 km. With regard to the brighter stars, these totals indicate that the following comments should hold for normal scattering conditions and no optical aid at a satellitic observation point:

1. For a surface grazing ray, the only objects surpassing in brightness the minimum magnitude of +6.0 for visual sighting are the Sun and the Moon.

2. For a ray with minimum tangent height of 5 km, the 5 brightest planets and 15 stars are also detectable.

3. For such a ray at 10 km, the number of available stars approaches 300.

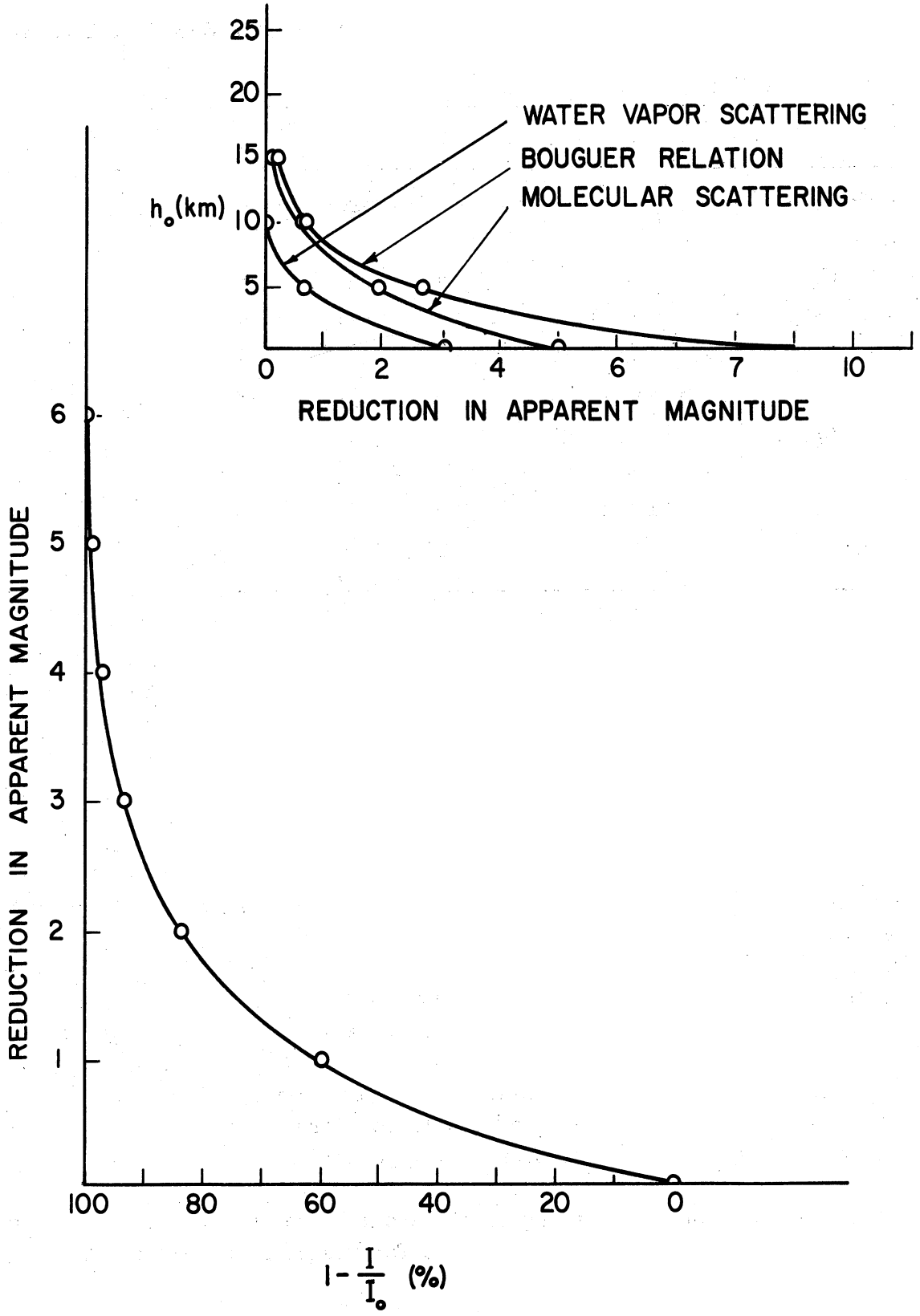

Fig. B-4. Reduction in apparent magnitude of stars as a function of attenuation $1 - I/I_0$.

TABLE B-VIII

REDUCTION IN APPARENT MAGNITUDE OF A HORIZONTAL RAY DUE TO ATTENUATING AGENTS, FOR $\lambda = 0.4\ \mu$ to $\lambda = 0.7\ \mu$

	h_o (kilometers)					
	0	5	10	15	20	25
(1) Refraction effect	2.6	2.1	1.6	1.1	0.6	0.2
Scattering						
Molecular	5.0	2.0	0.6	0.1	0.0	0.0
Water vapor	3.1	0.7	0.0	0.0	0.0	0.0
Haze and dust	3.9	0.2	0.0	0.0	0.0	0.0
(2) Bouguer Relation	10.0	2.7	0.7	0.2	0.0	0.0
Total of (1) and (2)	12.6	4.8	2.3	1.3	0.6	0.2

From the totals in Table B-VIII and a table of apparent stellar magnitudes, Fig. B-5 is obtained to show the number of stars detectable, theoretically, with no optical aid at the satellite and with instrumentation giving 2 and 4 magnitudes gain due to magnification. It is also interesting to note the number of stars which can be seen at the horizon, theoretically, by an observer situated at various levels within the atmosphere. In this case, one can omit the refractive attenuation and assume that the unaided eye can detect stars brighter than magnitude +6.0 with no scattering. Taking scattering into account as was done in Table B-VIII, the results are as shown in Table B-IX:

TABLE B-IX

NUMBER OF STARS THEORETICALLY DETECTABLE AT VARIOUS LEVELS WITHIN THE ATMOSPHERE, WITH SCATTERING TAKEN INTO ACCOUNT

h_o (kilometers)	Reduction in Magnitude Due to Scattering	Number of Stars Detectable
0	5.5	8
5	1.5	780
10	0.3	3400

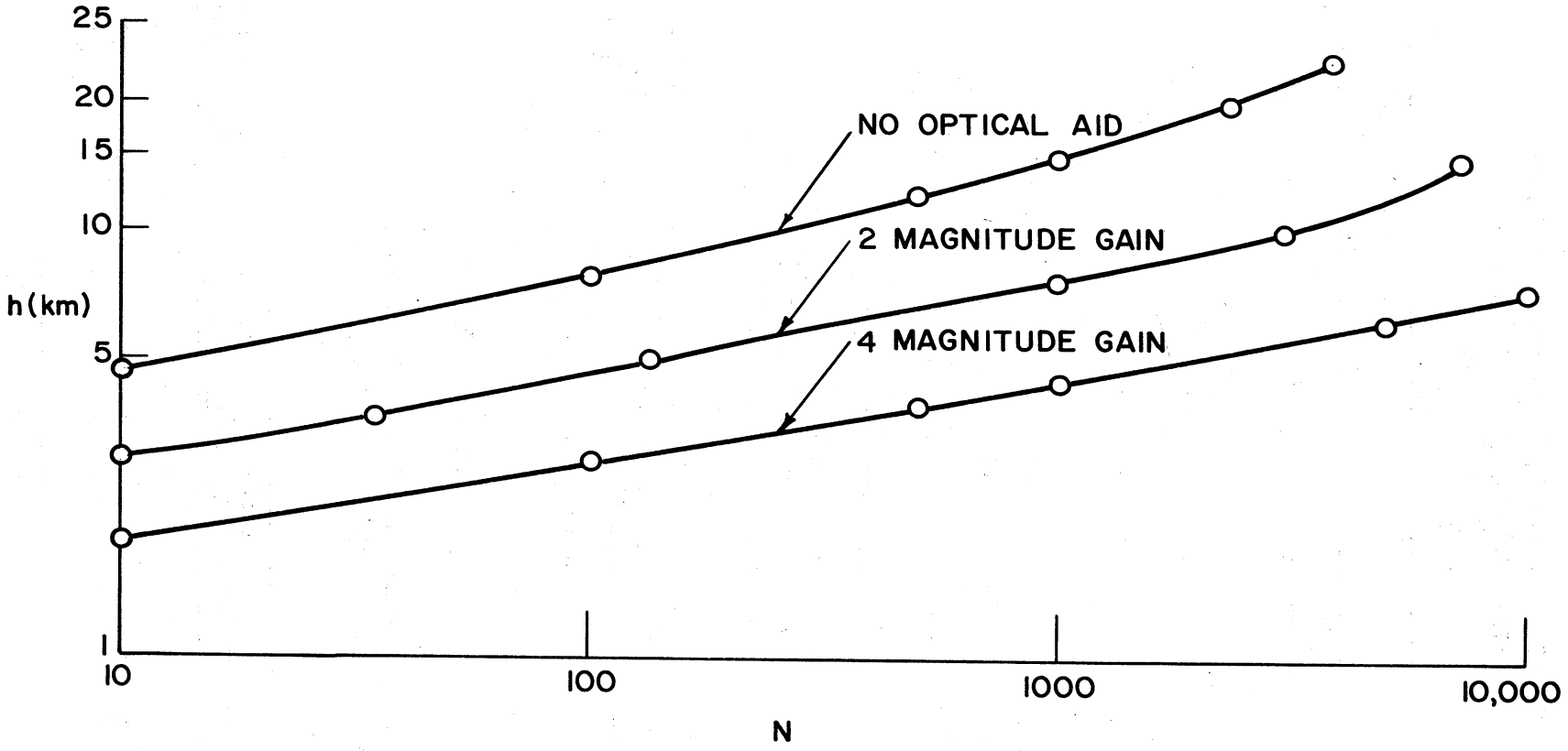

Fig. B-5. Number of stars theoretically detectable from a satellite with varying gains, as a function of ray perigee h_o.

The number of detectable stars is much greater in this case, due to the halving of the number of optical air masses traversed by the light ray and the elimination of refractive attenuation.

The distributions of some of the important variable scattering agents discussed in this report are not well known. In general, their influence in the upper troposphere is felt in tropical regions mainly, and in midlatitudes secondarily. The high extinction rates of clouds, for example, are of especially great importance near the intertropical Convergence Zones and around tropical disturbances. The frequency of occurrence of cirriform clouds range from 15 to 30% outside of these regions with a modal height of 7-10 km.

REFERENCES

1. Appleman, H. S., Occurrence and forecasting of cirrostratus clouds, Technical Note No. 40, WMO, Geneva, Switzerland, 1961.

2. Boll, Leacock, Clark and Churchill, Light-scattering functions, Univ. of Michigan Press, 1958.

3. Fowle, F. E., The atmospheric scattering of light, Smithsonian Misc. Collection, 69, No. 3, 1918.

4. Johnson, J. C., Physical Meteorology, M.I.T. and John Wiley and Sons, 1954, pp 33-64.

5. Jones, L. M., F. F. Fischbach, and J. W. Peterson, Atmospheric measurements from satellite observations of stellar refraction, University of Michigan Technical Report No. 04963-1-T, Jan. 1962.

6. Junge, Changnon and Manson, Atmospheric aerosols, J. Meteorology, Feb. 1961, pp 81-108.

7. Lillestrand, R. et al., Mechanical Division of General Mills, Inc., Minneapoli Minn., 1960.

8. Link, M. F., Occultations et eclipses des planetes, Bull. Astronomique, 9, 1933, p 227.

9. List, R. J., Smithsonian Meteorological Tables, Washington, D. C., 1958.

10. Mason, B. J., The physics of clouds, Oxford Monographs on Meteorology, London, 1957.

11. Middleton, W.E.K., Vision Through the Atmosphere, University of Toronto Press, 1952.

12. Moon, P., Proposed standard radiation curve for engineering use, J. Franklin Inst. 230, 1940, 588-593.

13. Pressly, E. C., Air mass between an observer and outer space, Physical Review, 89, No. 3, Feb. 1, 1953, 654-655.

14. Schoenberg, E., Handbuch der Astrophysik, Band II, Julius Springer, Berlin, 1929, 171-227.

15. Smithsonian Institution, Annals of Astrophysical Observations, 2, 1908, 113.

16. Stone, R. G., A compendium on cirrus and cirrus forecasting, AWS TR-105-130, USAF, 1957.

17. Van de Hulst, H. C., Light Scattering by Small Particles, John Wiley and Son, New York, 1957.

18. Van de Hulst, H. C., The Atmospheres of the Earth and Planets, The University of Chicago Press, 1952, 49-111.

19. Waldram, J. M., Measurement of the photometric properties of the upper atmosphere, Trans. of the Illuminating Engr. Soc., London, Aug. 1945.

APPENDIX C

VARIABILITY OF STARLIGHT DUE TO THE EARTH'S ATMOSPHERE

by Maurice E. Graves

I. INTRODUCTION

When a beam of starlight reaches the earth's atmosphere, its speed suffers a minute reduction and the light ray bends toward greater medium density. The wavefront, after being planar in space, undergoes corrugation when it passes through a layer of temperature inhomogeneity, and normal lines to the wavefront are no longer parallel (see Fig. C-1). To an observer of these nonparallel rays there may be fluctuations in image position, size and intensity, and distortion of image shape.

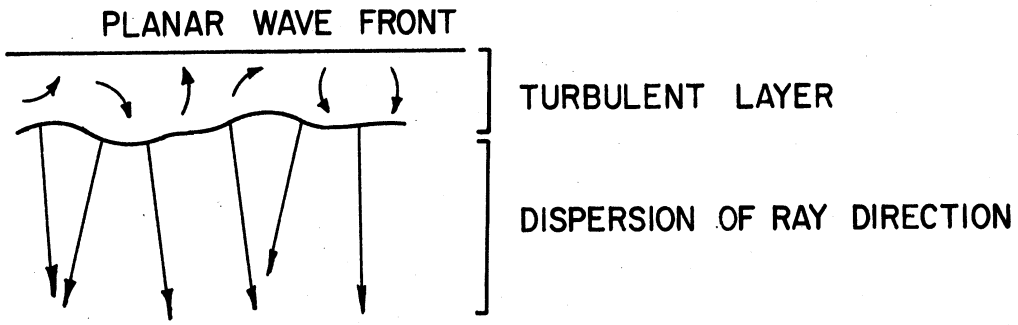

Fig. C-1. Dispersion of light rays upon passage through a turbulent layer in the atmosphere.

This report will summarize some of the literature dealing with fluctuation and distortion phenomena, and will make some estimates for horizontal grazing rays passing through the stratosphere and upper troposphere. The general procedure will be to condense the abundant information on stars observed near the zenith, to discuss the very limited material on stars with large zenith angles, and then to surmise what results may be expected for stars with large zenith angles viewed from high levels (see Fig. C-2).

A planetary atmosphere changes the intensity of a light ray as well as the direction of advancement, and it is convenient to speak of a "semi-constant" and a variable component for each, thus:

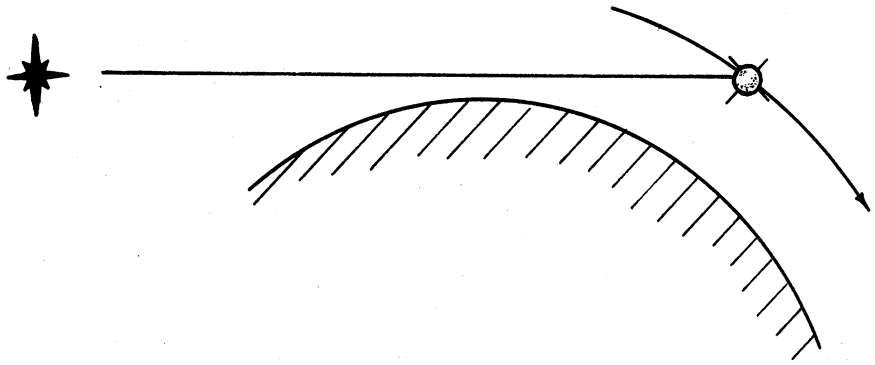

Fig. C-2. Simplified geometry of horizontal grazing ray viewed from satellite.

Change of direction	"semi-constant" term: refraction variable term: seeing (quivering distortion, pulsation)
Change of intensity	"semi-constant" term: extinction (scattering, absorption) variable term: scintillation

Besides the aperiodic variations of the magnitudes of the changes of direc-, there are large-scale seasonal, latitudinal and diurnal effects incorporated within the "semi-constant" term which are related directly to the temperature and density structure of the atmosphere.

II. SEEING

There is some overlapping of terms currently being used to describe the fluctuation of starlight. In this paper, the definitions used by Stock and Keller[14] and Tatarski[21] will be accepted as recent and authoritative, and parentheses will be used at times to signify related terms not appearing in these references. Thus the three basic image changes and movements will be referred to in the following ways:

1. Variation of magnitude: scintillation, twinkling
2. Variation of image size: distortion, pulsation, spreading, blurring
3. Displacement of image: quivering,

   (2) and (3), combined: seeing, poor seeing

Three major factors determine the quality of seeing for a particular stellar object:

1. Telescopic aperture, D
2. Meteorological conditions
3. Zenith distance, z

These factors will now be discussed in some detail.

At a particular time, a small D of, say, 10 cm employed at the ground will receive nearly parallel rays and form a relatively sharp image. However, at a later time, the parallel rays may have a slightly different direction, producing an image displacement. Rapid changes in the direction of the incoming rays cause an erratically moving image; this motion is called quivering (dancing).

On the other hand, a large D of, say, 30 cm may cover the entire range of ray directions, with the average direction being parallel to the wavefront. This gives a steady position, e.g., little quivering, but causes some distortion, e.g., spreading and blurring, amounting to an image diameter of 2-4" arc (see Fig. C-3).

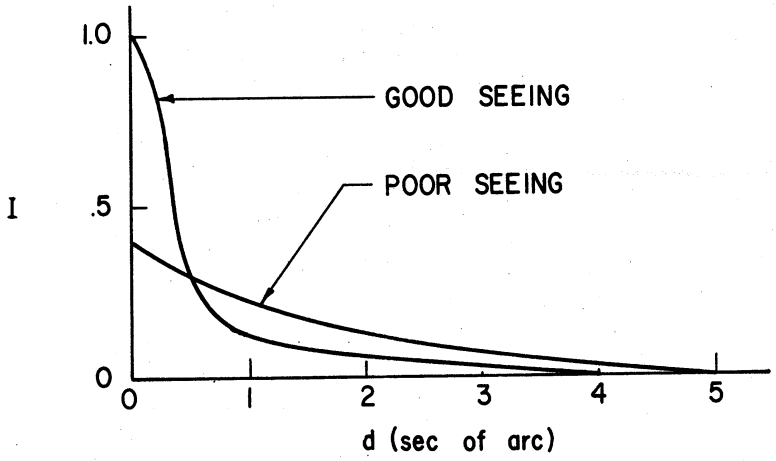

Fig. C-3. Image intensity I as a function of image diameter for typical cases of good and poor seeing.

For a given D and z, the seeing is determined by the meteorological conditions, specifically, the presence of temperature (and density) irregularities in horizontal planes. Seeing may originate anywhere in the atmosphere, but since density (and refractive power) decrease with altitude, the source of this type of fluctuation is more likely to be found in the lower levels. Within a turbulent zone near the ground, the eddy cells will act as lenses if their horizontal dimensions are no larger than D. Larger cells act as prisms, so the eddy effects are to encourage blurring in the first case and quivering in the second case. The prisms must change in shape or strength as the ray passes, however, if an image movement is to occur.

An expression related to the quality of seeing[14] is:

$$K^2 = \frac{2\pi^3}{\lambda^2} NL_m^2 \delta^2 f$$

where

λ = wave length of light;

N = average number of turbulent elements in path;

L_m = average size of elements;

$\delta^2 f$ = mean square variation of μ, the refractive index.

When $K^2 < 1$, the quality of seeing is good, that is, any turbulent layer permits the light to pass through in an undiffracted (zero-order) plane wave.

When $K^2 > 1$, the quality of seeing is inferior.

It should be noted here that δf in the above expression is simply the difference between the refractive index of the air inside a turbulent element and the refractive index of the environment, thus:

$$\delta f = \frac{\delta \rho}{\rho_o} (\mu_o - 1)$$

where subscript zero refers to ρ and μ at normal T and p.

But $p = \rho RT$, where p, ρ and T refer to environment air

$$0 = \delta p = \delta\rho(RT) + (\rho R)\delta T$$

$$\frac{\delta \rho}{\rho} = -\frac{\delta T}{T}$$

$$\delta f = \frac{\delta \rho}{\rho_o} (\mu_o - 1) = -\frac{\rho}{\rho_o} \frac{\delta T}{T} (\mu_o - 1)$$

Near sea level, $\mu_o - 1 = 2.9 \times 10^{-4}$ and $\delta f = -1 \times 10^{-6} \delta T$.

It is clear that an increase in zenith distance, z, leads to a notable increase in path length of a starbeam passing through the atmosphere. This leads one to expect a positive change in any of the fluctuations when z nears 90°. Tatarski[21] has published Russian work on quivering which shows the rms magnitude

to be less than 1" arc for $z < 85°$ (see Fig. C-4). The frequency of image movement is not discussed therein, but Ellison and Seddon[5] state that the frequency of quivering is similar to that of scintillation.

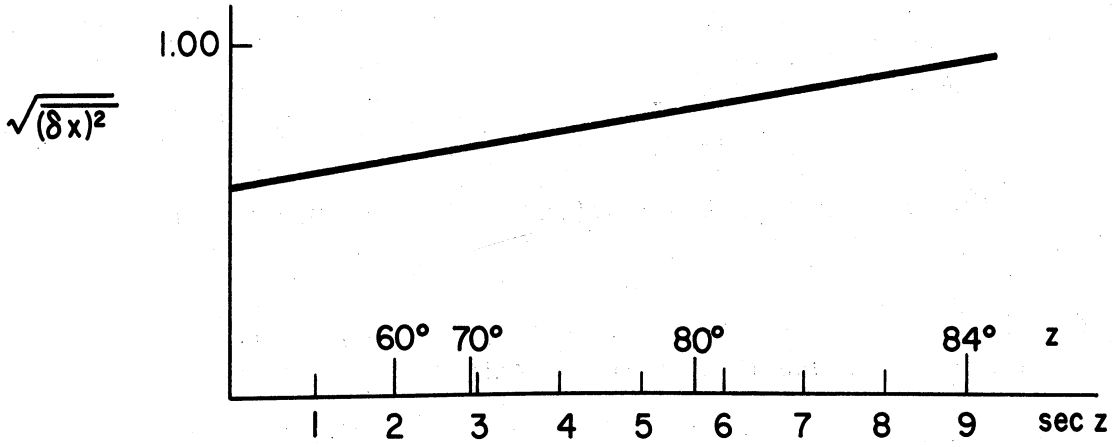

Fig. C-4. RMS fluctuations of starlight as a function of zenith angle z, for $z < 85°$.

For a horizontal path through the entire atmospheric shell tangent to the earth's surface, the rms magnitude must be increased. Since the path length is thereby doubled, the application of the principle of discontinuous, random motion in one dimension gives a factor of $\sqrt{2}$. Therefore, the quivers would have a total rms magnitude of about 1.0" x $\sqrt{2} \approx 1.5$" at zenith angles of 60-85° and about double this amount at z close to 90°. The following calculation gives the percentage rms error at the surface:

$$\frac{3\text{" arc}}{69' \times 60"/1'} = 0.1\%$$

Here, 69' is the representative refraction angle for a complete path.

Although the prism-like segments of larger eddies lose their importance to seeing above lower levels, there is some question about horizontal layers in the turbulent wind shear zones near jet streams. When considering a large z and small D in viewing through such a layer, it appears that some quivering will take place when large eddies are present. On the other hand, the following computation indicates that the percentage error is again very small:

Let R_s = refraction angle for a complete horizontal traverse

$$(R_s)_{12\ km} = 18'$$

$$(R_s)_{sfc} = 69'$$

$$\frac{(R_s)_{12\ km}}{(R_s)_{sfc}} = \frac{1}{4}$$

Let ρ = air density

$$\frac{(\rho)_{12\ km}}{(\rho)_{sfc}} = 0.3$$

The ratio $R_s/\rho \approx$ a constant below 12 km and the percentage error due to quivering remains at 0.1% when the prism-like eddy segments maintain the same frequency of occurrence and variability throughout the troposphere.[11] The turbulent layers aloft will be taken up again in Section IV.

III. EXTREMES OF SEEING

Seeing encompasses both quivering and image distortion, and its extreme form is pulsation. Tombaugh,[22] in gusty surface wind conditions, has recorded the swelling of 3rd magnitude δ Geminorum to three or four times the size of Jupiter. The swelling was followed by total disappearance in the telescope for several seconds.

Notwithstanding this reported case of pulsation, there is no evidence that large variations in image size, and disappearances in particular, occur during normal viewing, even at surface air density.

The individual extreme values in quivering are not given in Tatarski,[21] but they may be estimated from the rms when one assumes a certain number of observations, thus:

$$\Pr\left[a < \frac{x - \bar{x}}{\sigma/\sqrt{n}}\right] = \Pr\left[\frac{a\sigma}{\sqrt{n}} < x\right]$$

where

a = an arbitrary extreme value

$\bar{x}$ = mean = 0

n = number of observations

Now suppose σ = rms = 3" and n = 100; these assumptions give the following percentage probabilities (see Table C-I) that a quiver will exceed an extreme value, a:

TABLE C-I

PROBABILITY OF EXCEEDING VARIOUS EXTREME VALUES OF QUIVERING

a(" arc)	Pr [x > a] (%)
4	11.51
6	3.59
8	0.82

IV. SCINTILLATION

Scintillation* was introduced above as a variable quantity associated with change of starlight intensity. More specifically, it is definable as the frequency of stellar magnitude variations. Its observable effects and its causes will be discussed as we take up again the three major factors which were important to the quality of the seeing, and which also determine the scintillation, namely:

1. Telescopic aperture
2. Meteorological conditions
3. Zenith distance

There has been considerable discussion, even controversy, about the optical nature of scintillation. Rayleigh[20] was one of the early investigators in this field, with his refraction theory in 1893. His results indicated that the altitude of scintillation origin was less than 4 km. Later, Little[15] criticised this theory and introduced his diffraction theory. Little's most effective criticism was that in the refraction theory, the density gradient must be of the order of magnitude of 0.5%/cm, a figure which is far greater than what may reasonably be expected in the upper troposphere. The diffraction theory, on the other hand, needs but 0.0006%/cm gradient, which corresponds to 0.002°C/cm temperature gradient. Diffraction, however, seems to require a rather thick disturbing layer, according to Little, whereas refraction theory conforms well to the notion of a thin-layered scintillation source region.

Although challenged on several points, it appears that Fellgett's discussion[7] of the two theories explains the basic differences. Starting with the postulate that scintillation deals with the propagation of light through an atmosphere of varying refractive index, it is clear that one is dealing with the wave properties of light. A boundary-value solution of Maxwell's Equations would be desirable, but this is so complex a problem one seeks an approximation. The

*We are concerned here with brightness scintillation, and will ignore the second type, called chromatic or color scintillation.

first-order approximation is Huygens' Principle of propagation of light waves, and diffraction enters into the application. The second-order approximation assumes that wave length is negligible in magnitude and no diffraction occurs. It is commonly referred to as the "Ray Theory," and is in the field of geometric optics; Huygens' Principle is in the field of physical optics.[10] The former model is adequate for most considerations, but wave diffraction techniques give more realistic results at times and their theoretical base is more rigorous.

During the past 15 years, there have been a number of studies on the nature of scintillation, e.g., its observed effects, frequency, origin, etc., by Chandrasekhar,[4] Ellison and Seddon,[5] Epstein,[6] Gaviola,[8] Keller,[12,13] Mikesell, Hoag and Hall,[16] Protheroe,[18,19] and Tatarski.[21] Before considering the three determining factors explicitly, some attention will be given these facets of the subject.

The principal observable effect is the shadow-band of about 8 cm band-width. Shadow-bands form transitory patterns, due to their rapid motion and structural changes. They move in accordance with the wind at their level of origin, leading to some successful efforts[19] to find the wind speed at an assumed altitude, usually near the tropopause.* The formula $V = aR^b$ gives a good fit between the desired wind speed aloft, V, and the scintillation ratio, R (300 cycle/sec component/10 cycle/sec component). For single frequencies, Gifford[9] has shown that the 150 cycle/sec scintillation frequency has its maximum correlation with wind speed at 30-40,000 feet, but the 9 cycle/sec frequency has little correlation below 60,000 feet.

Lord Rayleigh's question,[20] "Is the ultimate effect (of scintillation) a small residue of neutralizing effects?" has been answered negatively by all investigators who have been active in the field in the past few years. In fact, there is ample evidence that the shadow-bands are related to wind velocity near 10 km;[1,6,19] furthermore, they are inclined identically to the Fraunhofer lines, so that a single height or thin layer is the cource of the intensity variations. Meinel[14] states that the minimum thickness of this layer is 10 cm.

Photomultiplier tubes have been used by Barnhart, Keller, and Mitchell,[1] Keller,[13] Mikesell, Hoag and Hall,[16] and Protheroe,[18,19] to study the shadow-bands. The schematic diagram in Fig. C-5 illustrates the method employed in conjunction with an analog computer.

Whereas the unaided eye detects the lower range of frequencies up to 16 cycle/sec, the instrumental readings give values up to 1000 cycles/sec.

The specific cause of scintillation is necessarily a phenomenon which creates multiple refractions. The sole candidate appears to be turbulence, e.g., the eddy motion of parcels of air with differing indices of refraction.

*Although the singular form of "tropopause" is used here, duplicity is not uncommon, especially near jet stream cores and in the subtropics.

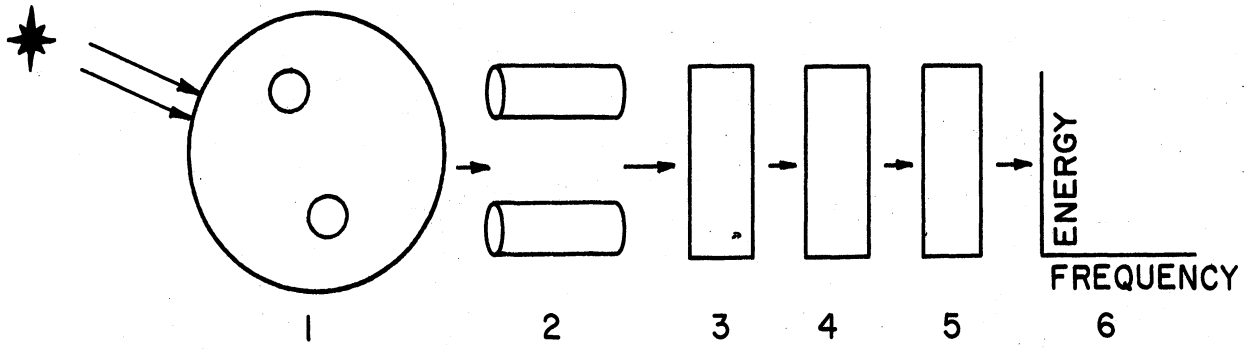

Fig. C-5. Photomultiplier tube as used to obtain Fourier spectra for scintillation.

1. Objective lens with twin, rotatable apertures
2. Two photomultiplier tubes
3. Analog computer
4. Autocorrelation coefficients obtained
5. Autocorrelation function obtained
6. Fourier spectra obtained

This eddy motion is also the cause of aircraft turbulence, and since the advent of jet-turbine engines at least a start has been made toward the discovery of its distribution in space. In general terms, we may say that the altitude of origin is usually near the tropopause, where wind speed, wind shear (in any plane) and the vertical density gradient can be relatively large at times. This altitude ranges as shown in Table C-II.

TABLE C-II

RANGE OF MEAN TROPOPAUSE ALTITUDES

Latitude	Altitude of Mean Tropopause
0 - 25°	16 km
25 - 60	10 - 16
60 - 90	8

It is interesting to compare Table C-II with Table C-III, which shows irregularities obtained by checking the transitional motion of the shadow-bands against observed winds.

TABLE C-III

ALTITUDE OF DENSITY IRREGULARITIES
AS OBTAINED BY VARIOUS INVESTIGATORS

Year	Investigator	Altitude of Density Irregularities; Basis
1893	Rayleigh[20]	4 km; refraction theory
1952	Ellison and Seddon[5]	5 km; planetary scintillation
1954	Barnhart, Keller and Mitchell[1]	11 km; observed winds versus transitional motion of shadow patterns
1954	Epstein[6]	10 km; ditto
1955	Protheroe[18]	9 km; ditto
1961	Protheroe[19]	9 km; ditto

The altitude values of 9-11 km appearing in Table C-III approximate the level of typically strong wind shear just below the tropopause around organized jet streams. They also approximate tropopause altitude in midlatitudes when the tropopause is at maximum depression.

The first of the three major factors determining scintillation is telescopic aperture. Perhaps the simplest way to express the relationship is as follows:

Random statistical fluctuations, viz. scintillation,

$\propto (A)^{-1/2}$, where A = aperture area

Aperture diameter $D \propto A^{1/2}$

Thus scintillation $\propto (D)^{-1}$. Since quivering is also a random fluctuation, the magnitude of image displacements $\propto (D)^{-1}$. A similar result can also be obtained from an analysis of the spectrum function (see Fig. C-5).[1]

Table C-IV summarizes some of Protheroe's results[19] and it shows the contrast between small and large apertures, with zenith angle = 0°:

The meteorological conditions attendant to pronounced scintillation must be those which produce turbulence at altitudes near 10 km, for turbulence has been designated as the sole cause and the evidence to date favors such altitudes. The eddy motion in the wind shear zones mentioned above is known to be strong at times, and of suitable eddy size to cause significant bumpiness in jet aircraft moving at about 300 mps. This eddy size would be of magnitude

TABLE C-IV

FOURIER SPECTRA RELATED TO FREQUENCY RANGES AND APERTURE SIZE

Aperture Diameter	Frequency	Strength of Fourier Spectra
1-3 in.	0-100 cy/sec	About constant
1-3	100-500	Transitional
1-3	500-1000	About zero
10-20	10-50	About constant
10-20	50-100	Transitional
10-20	100-500	About zero

several tens to a few hundred meters. However, we know that we must deal with density irregularities of only a few centimeters magnitude, for planets show little tendency to scintillate when their diameters are as great as 30" arc.[12] At 10 km, 30" arc corresponds to just 5 cm.*

The aircraft observations of turbulence establish the occasional presence of large eddies and the fact that the turbulent layer is usually evaded by the customary 600-meter change in flight altitude. In addition, the writer has often noticed shear-produced "Cobblestone Turbulence" in jet aircraft, and the eddy sizes would be in the range of several meters to a few tens of meters in these cases. Employing Kolmogoroff's ideas on eddy energy dissipation,[2] one can easily visualize a spectrum of eddy sizes ranging on down to zero diameter, thus accounting for the necessary scintillation source, e.g., eddy sizes of 5 cm or less.

The importance of zenith angle, z, can be seen by examining the spectrum function (see Fig. C-5). This may be written as:[14]

$$\frac{B(w)}{h_o^2} = \frac{16\pi^2 \Delta z b(w) \sin^2(\pi z \lambda w^2)}{\lambda^2}$$

where

$B(w)$ = spectrum function for the shadow pattern

h_o^2 = mean square amplitude of intensity variation in pattern

*The Ellison and Seddon result of 5 km in Table C-III is based upon a much smaller maximum planetary scintillation diameter, of but 3". It assumes an average eddy diameter of 8 cm, equal to the average width of shadow-bands. The writer feels that 3" is much too small, and that 30" is about right for the critical arc length.

Δz = slant distance through layer

$b(w)$ = spectrum function for the frequency of elements of different sizes

z = slant distance from telescope to turbulent layer

λ = wave length in cm

w = wave number (1/cm)

The turbulence is assumed to be homogeneous and isotropic, and these assumptions seem to be satisfied quite well in natural conditions, excepting very near the earth's surface.

When z is quite large, the $\sin^2(\pi z \lambda w^2)$ term begins to oscillate between 0 and 1, but Δz increases, so that $B(w)$ must tend to increase or h_o^2 must decrease, or both. The latter quantity does decrease slightly, and this is confirmed by Tatarski,[21] who states that a chromatic effect sets in at $z = 60°$ whereby the scintillation at different wave lengths loses its correlation, producing a lessening of total twinkling effect as z increases further. However, large amplitude, low frequency oscillations increase at low star altitudes, as we can readily observe by using the unaided eye in the visual range. Some values for range/mean of the total amplitude of stars at $z = 0°$ and $z = 90°$ are given by Protheroe[19] for a small aperture:

TABLE C-V

RANGE/MEAN OF TOTAL AMPLITUDE
OF STARS AT $z = 0°$ AND $z = 90°$

D	z	Range/mean
1-3 in.	0°	.5-1.5
1-3 in.	90°	About 10

Thus, for small apertures, the total amplitude of the fluctuations increases by a whole order of magnitude when z approaches 90°. With larger apertures, the amplitude gain is not as great.

For a horizontal path near the earth's surface, using a light source at a finite distance, Project Michigan investigators[3] have shown scintillation-dependence mainly upon the vertical temperature gradient and the turbulence characteristics along the path, but also upon the path length and wind speed and direction. If a surface temperature inversion is present, a fair amount of mixing produces strong scintillation.

Above the low-level zone where the above type of scintillation is detected, the occurrence of this phenomenon through a horizontal path is not well known. Meinel[14] mentions manned balloon ascents where diminishing scintillation effects were observed through the first 6 km, with negligible fluctuations of any kind above 15 km. There is little indication of the amount of scintillation one perceives when passing through the tropopause layer or a wind shear zone where the meteorological conditions are likely to encourage its occurrence. If we assume the tropopause to be parallel to the earth's surface in all directions in the neighborhood of a data point, then the maximum distance traversed by an unrefracted light ray within such a layer is related to the layer thickness, Δz (see Fig. C-6). An analytical solution gives the values shown in Table C-VI.

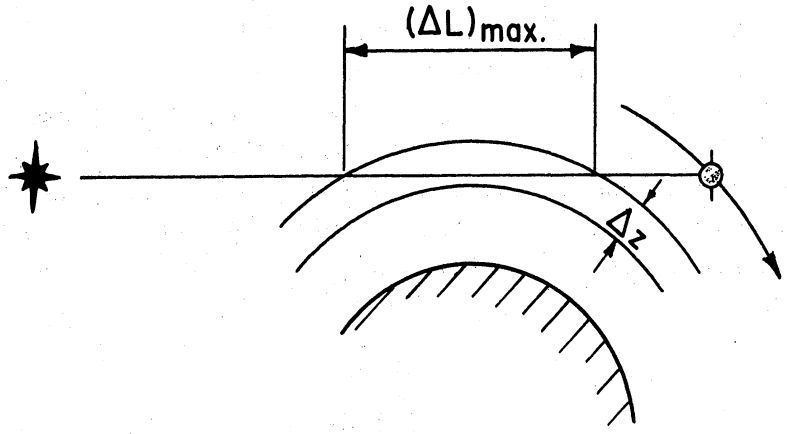

Fig. C-6. Simplified geometry of maximum distance traversed by a straight horizontal ray.

TABLE C-VI

MAXIMUM DISTANCE TRAVERSED BY A STRAIGHT HORIZONTAL RAY WITHIN A LAYER Δz, FOR VARIOUS LAYER THICKNESSES

Δz	$(\Delta L)_{max}$
100 mt	74 km
250	112 km
500	160 km
750	196 km
1000	226 km

Several minor causes have been omitted from this discussion of scintillation and seeing. Water vapor, for example, has a high opacity for infrared radiation, giving it a greater influence than would be estimated from the refractive index of moist air. The mechanism producing temperature and density irregularities is the radiation loss of heat from moist air masses at night, into space. Five km may be a reasonable estimate of the tops of the moist layers in most air masses of this type.

Second, Minnaert[17] refers to the relation of scintillation to path water content, cloud edges, isobar curvature and low-level gradients of temperature, density and pressure, but all of these possible causes can be discounted in tangential star-tracking above a few km.

Third, the differing physical properties of stars are responsible for scintillation anomalies. One qualitative statement citing such differences is a law of Bijourdan[23] which states that the spectral range of a star decreases from white to red, thereby reducing the scintillation in a like manner.

V. CONCLUSIONS

Variations in the direction of motion and in the intensity of a starbeam fall into the general categories of seeing and scintillation, respectively. In either case, the major factors which determine the amount of observed variation are (1) telescopic aperture, (2) meteorological conditions and (3) zenith distance.

Increase of aperture reduces quivering, which is the principal seeing phenomenon, but it distorts the image shape so that a stellar point image then attains a diameter of 2-4" of arc. Increase of aperture also reduces scintillation, beginning with the higher frequencies.

Meteorological turbulence, producing prism-like segments which momentarily deflect light rays, is the basic cause of seeing. Near the ground, but probably not aloft, such turbulence sometimes causes changes in image size, called pulsation. Studies of the shadow-bands of scintillation have established high-level turbulence near the tropopause as the chief source of this effect.

The additional path length for zenith angles near 90° increases quivering to an rms value of about 3" arc for a complete traverse, but the resulting angular error is only 0.1%. With small apertures, total scintillation amplitude increases by a factor of 10 at these zenith angles, with larger apertures increases somewhat less.

At minimum grazing distances of several kilometers, the seeing error should not exceed its surface magnitude of 0.1% and the scintillation effect may be expected to decrease with altitude due to decrease of the air density. However, in turbulent inversion layers such as those commonly encountered near the tropo-

pause at about 10 km, grazing angles will evidently have horizontal path segments of a few kilometers lying within the perturbed zones. At these particular levels, there is a strong possibility of significant scintillation effects when there is turbulence.

REFERENCES

1. Barnhart, P. E., G. E. Keller, and W. E. Mitchell, Jr., Investigation of upper air turbulence by the method of analyzing stellar scintillation shadow patterns, Final Technical Report, Air Force Cambridge Research Center and The Ohio State U. Research Foundation, July 1959.

2. Batchelor, G. K., Quart. J. Roy. Meteorol. Soc., 76, 133-146, 1950.

3. Bellaire, F. R., and F. C. Elder, Scintillation and visual resolution over the ground, Willow Run Laboratories, The University of Michigan, October 1960.

4. Chandrasekhar, S., Monthly Notices Royal Astron. Soc., 112, 473-483, 1952.

5. Ellison, M. A. and H. Seddon, Monthly Notices Royal Astron. Soc., 112, 73-87, 1952.

6. Epstein, E. S., Relation between stellar scintillation and atmospheric phenomena, The Pennsylvania State University, Unpublished Master's Thesis, June 1954.

7. Fellgett, P. B., Quart. J. Royal Meteorol. Soc., April 1956.

8. Gaviola, E., On seeing, fine structure of stellar images, and inversion layer spectra, The Astronomical Journal, 54, 155-161, 1949.

9. Gifford, F., Jr., Bull. American Meteorol. Soc., 36, Jan. 1955.

10. Humphreys, W. J., Physics of the Air, McGraw-Hill Book Co., Inc., New York, 1929.

11. Jones, L. M., F. F. Fischbach, and J. W. Peterson, Atmospheric measurements from satellite observations of stellar refraction, Technical Report, The University of Michigan, January 1962.

12. Keller, G. E., Astronomical "seeing" and its relation to atmospheric turbulence, The Astron. J., 58, 113-125, July 1953.

13. Keller, G. E., Relation between the structure of stellar shadow band patterns and stellar scintillation, J. of the Opt. Soc. of America, 45, 845-851, October 1955.

14. Kuiper, G. P. and B. M. Middlehurst, Telescopes, The University of Chicago Press, Chicago, Ill., 1960.

15. Little, C. G., A diffraction theory of the scintillation of stars on optical and radio wave-lengths, The Roy. Astron. Soc. Monthly Notices, 111, 289-302, 1951.

16. Mikesell, A. H., A. A. Hoag, and J. S. Hall, The scintillation of starlight, J. of the Opt. Soc. of America, 41, 289-295, Oct., 1951.

17. Minnaert, M., The Nature of Light and Colour in the Open Air, Dover Publications, Inc., New York, 1954.

18. Protheroe, W. M., Determination of shadow band structure from stellar scintillation measurements, J. of the Opt. Soc. of America, 45, 851-855, October, 1955.

19. Protheroe, W. M., Stellar scintillation, Science, 134, 1593-1599, 17 November 1961.

20. Rayleigh, Lord, On the theory of stellar scintillation, Philosophical Magazine S5, 36, 129-142, July 1893.

21. Tatarski, V. I., Wave Propagation in a Turbulent Medium, McGraw-Hill Book Company, New York, 1961.

22. Tombaugh, C. W. and B. A. Smith, A seeing scale for visual observers, Sky and Telescope, XVII, 449, July 1958.

23. Vassy, E., Physique de L'Atmosphere, Vol. II, Gauthier-Villars, Paris, 1959.